A Coupled Map Lattice Model of Flow Boiling in a Horizontal Tube
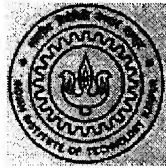
A Thesis Submitted

in Partial Fulfillment of the Requirements

for the Degree of

Master of Technology

by

Indrajit Chakraborty

to the

Nuclear Engineering and Technology Programme

Indian Institute of Technology Kanpur

India

A Coupled Map Lattice Model of Flow Boiling in a Horizontal Tube

A Thesis Submitted

in Partial Fulfillment of the Requirements

for the Degree of

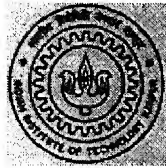## Master of Technology

by

Indrajit Chakraborty

to the

Nuclear Engineering and Technology Programme

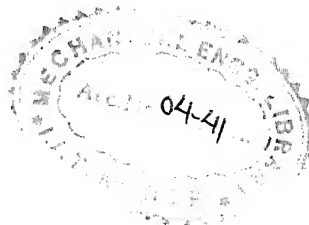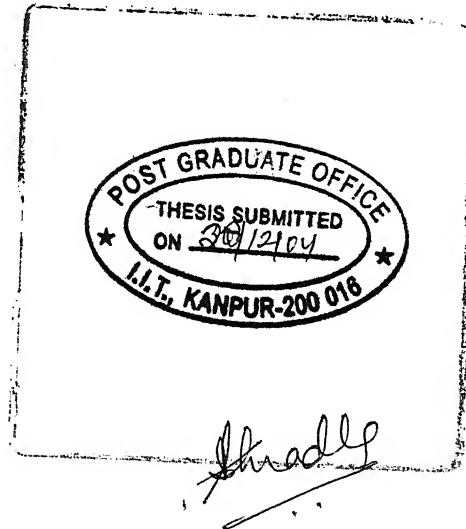## Indian Institute of Technology Kanpur

India

CERTIFICATE

It is certified that the work contained in the thesis entitled, **"A Coupled Map Lattice Model of Flow Boiling in a Horizontal Tube"** by **Indrajit Chakraborty** (Y221501) has been carried out under my supervision and this work has not been submitted elsewhere for a degree.

P.S. (a dust

Dr.P.S.Ghoshdastidar
Professor
Department of Mechanical Engineering
Indian Institute of Technology Kanpur

December, 2004
Kanpur

Acknowledgements

CONTENTS

:

List of Figures

vi

Abstract

In this work laminar (that is, laminar liquid, laminar vapour) flow boiling of water as well as propane has been simulated qualitatively by a method known as the Coupled Map Lattice (CML) method. CML is a simple model introduced first in 1983 by Kunihiko Kaneko. The CML model has essential features of spatiotemporal chaos. Over the past two decades, studies of the CML have been expanding not only in the field of spatiotemporal chaos and pattern formation but also in the fields of biology, mathematics and engineering. In the area of pool boiling so far only four studies of CML have been reported. They are Yanagita (1992), Shoji and Tajima (1997), Shoji (1998) and Ghoshdastidar et al. (2004). So far no studies showing CML simulation of flow boiling have been found in the open literature. The present work is a first attempt in this direction.

A CML is a dynamical system with discrete-time, discrete-space and continuous states. It usually consists of dynamical elements on a lattice which interact (are 'coupled') with suitably chosen sets of other elements. The strategy of modelling dynamical phenomena in spatially extended systems by a CML model is based on the following steps.

1. Choose (set of) macroscopic variables on a lattice.

2. Decompose the processes underlying the phenomena into independent components.

3. Replace each component by a simple parallel dynamics on a lattice.

4. Carry out each unit dynamics (or procedure) successively.

The modelling by CML is based on the assumption that the flow boiling is governed by (a) nucleation from cavities on the heated surface (b) forced convection and (c) phase change in the fluid bulk and mixing. The macroscopic variable chosen is temperature. The problem is transient and marches to steady state solution. The forced convection part in CML part is solved using CFD techniques, assuming average properties of the fluid.

The main observations from the results are the following. (i) The wall temperature does not affect the heat transfer coefficient and vapour fraction; (ii) The decrease in entry subcooling lowers the heat transfer coefficient near the tube entrance but does not

influence the heat transfer coefficient in the latter part of the tube. Furthermore, vapor fraction is high near the tube entrance for low ΔT_{sub}'s whereas the maximum vapour fraction is same for all ΔT_{sub}'s. (iii) The heat transfer coefficient is virtually independent of mass flow rate in the initial section of the tube where the nucleate boiling effect is dominant. On the other hand, in the latter part of the tube where the convection vapourization is significant, heat transfer coefficient falls with increase in mass flow rate. All these trends are similar for both water and propane.

An exception for propane is noted where it is seen that fluid mean temperature is higher for $\Delta T_{sub} = 20°C$ than for $\Delta T_{sub} = 30°C$ in the section of the tube from z = 4.8m to 6m. Another difference with respect to water is that the convective vapourization zone is much larger as compared to the zone where the nucleate boiling is dominant. In addition to the above, the drop in heat transfer coefficient at some location down the tube is not as marked as that for water.

Nomenclature

last grid point number in the circumferential
direction

pressure (N/m^2)

wall heat flux (W/m^2)

random number between 0 and 1

Reynolds number ($\rho_{eq} v_m D / \mu_{eq}$)

radial coordinate (m)

radius of the cylindrical tube (m)

time (s)

increment

temperature (^0C)

nucleation wall temperature (^0C)

saturation temperature (^0C)

wall temperature(^0C)

mean temperature of fluid (^0C)

nucleation superheat $= T_{act} - T_{sat}$ (^0C or K)

level of subcooling (^0C), $T_{sat} - T_{mean}$

volume of liquid and vapour (m^3)

volume of vapour (m^3)

velocity (m/s)

mean velocity (m/s)

velocity (m/s) in axial direction

Cartesian coordinates

axial coordinate(m) i.e. along the tube axis

Greek Symbols	Description
β	maximum deviation from D_m (μm)
η	parameter in phase change or mixing
θ	circumferential coordinate (radian)
μ	viscosity (kg/m-s) or (N-s/m^2)
ν	kinematic viscosity (m^2/s)
ρ	density (kg/m^3)
σ	surface tension (N/m)

Subscripts

entrance	tube inlet
eq	equivalent
f	fluid
l	liquid
m	minimum
sat	saturation
lam	laminar
v	vapour
mean	mean value

Superscripts

p	at present time
p+1	at future time

Abbreviations

CFD	computational fluid dynamics
CHF	critical heat flux
CML	coupled map lattice
NAG	numerical algorithm group

CHAPTER 1

INTRODUCTION

1.1 Introductory Remarks

In this work laminar (that is, laminar liquid, laminar vapour) flow boiling of water as well as propane has been simulated qualitatively by a method known as the Coupled Map Lattice (CML) method. CML is a simple model introduced first in 1983 by Kunihiko Kaneko. The CML model has essential features of spatiotemporal chaos. Over the past two decades, studies of the CML have been expanding not only in the field of spatiotemporal chaos and pattern formation but also in the fields of biology, mathematics and engineering. In the area of pool boiling so far only four studies of CML have been reported. They are Yanagita (1992), Shoji and Tajima (1997), Shoji (1998) and Ghoshdastidar et al. (2004). So far no studies showing CML simulation of flow boiling have been found in the open literature. The present work is a first attempt in this direction.

A CML is a dynamical system with discrete-time, discrete-space and continuous states. It usually consists of dynamical elements on a lattice which interact (are 'coupled') with suitably chosen sets of other elements. The strategy of modelling dynamical phenomena in spatially extended systems by a CML model is based on the following steps.

1. Choose a (set of) macroscopic variables on a lattice.
2. Decompose the processes underlying the phenomena into independent components.
3. Replace each component by a simple parallel dynamics on a lattice.
4. Carry out each unit dynamics (or procedure) successively.

In the present study, the liquid is entering a constant wall temperature tube ($T_W > T_{sat}$) in a subcooled condition (Fig.1.1). The objectives of this study are to obtain qualitatively heat transfer coefficient, wall heat flux, mean fluid temperature, and vapour fraction as a function of axial coordinate.

The modelling by CML is based on the assumption that the flow boiling is governed by (a) nucleation from cavities on the heated surface (b) forced convection and (c) phase change in the fluid bulk and mixing. The macroscopic variable chosen

is temperature. The problem is transient and marches to steady state solution. The forced convection part in CML part is solved using CFD techniques, assuming average properties of the fluid.

The reason why CML is qualitative is because the actual governing equations are not solved. Ideally, a computational fluid dynamics study of flow boiling would be possible if the Navier-Stokes equation could be solved together with continuity and energy equations along with phase change and appropriate boundary conditions. However, there are several problems in simulating the flow boiling phenomena based on CFD. First, numerical instability will occur because the boundary of the two phases is complex and varies with time. Second, the amount of CPU time needed for the integration of the equations will be very large since the calculations need to be carried out with high accuracy to avoid such numerical instabilities. Furthermore, with the numerical techniques available at present only a few bubbles can be dealt with at best.

1.2 An overview of flow boiling

Boiling in forced flow is called flow boiling or convective boiling. Generally, in most vapour-producing equipment vapourization occurs under forced convection. The flow conditions are influenced to a great extent by the pressure gradient along the heating surface. The vapour content increases along the path of flow up to the point of complete vaporization. In general, a liquid enters in a sub-cooled condition into a heated channel. Vapour bubbles formed at the wall due to nucleation condense again in the colder core of the liquid. If the liquid in the core is heated up to saturation temperature, then saturated nucleate boiling results.

Figure1.2 shows the various regimes in succession in the flow boiling in a vertical heated tube. After the *bubbly* flow characterizating nucleate boiling the individual bubbles grow together into large bubbles, that is, they develop into a slug flow. With increasing vapour content the large bubbles also grow together so that at first there is *semi-annular* flow and, subsequently, there forms at the tube wall a liquid film and a vapour core with liquid drops which is called annular-*dispersed* flow. With further addition of heat, the liquid film disappears downstream and in this part the two-phase flow contains vapour with liquid drops. This regime is called *spray or mist*

flow. In most technical applications annular-dispersed flow occurs frequently. Slug flow occurs if the flow velocity is small.

We already know that in pool boiling the flow field and heat transfer are determined by the difference between the hot surface and saturation temperature, as well as by the properties of the fluid and the heating surface. On the other hand, in boiling in forced flow the velocities of the vapour and liquid phases and the distribution of phases are additional factors that influence the flow field and heat transfer. Therefore, in flow boiling the empirical heat transfer coefficient relationships are of the form $h = c (q'')^n (\dot{m}'')^s f(x^*)$, where $\dot{m}''$ and x^* represent the mass flux of the fluid and the vapour quality respectively. In nucleate boiling the heat transfer coefficient is chiefly dependent on the heat flux and practically not at all on the flow velocity. On the contrary, in convective boiling the heat transfer coefficient is primarily influenced by the velocity of the flow or by the mass flux but hardly by the heat flux. In flow boiling, n is nearly zero, s lies between 0.6 and 0.8, while in the nucleate boiling portion, $n = 0.75$ and s lies between 0.1 and 0.3.

For large Froude numbers, the flow regime is same both for vertical tube and horizontal tube, the reason being the forces of inertia are so great in comparison to the forces of gravity that no noticeable stratification occurs. With smaller Froude number, especially for $Fr < .04$, the stratification is very pronounced, and the influence of the slope of the tube must be considered. Fig. 1.3 shows various regimes of flow boiling in a heated horizontal tube for a non-stratified flow.

There are two types of flow boiling crisis. One is film boiling and other is dryout. In film boiling crisis, the critical heat flux is reached at very high constant wall heat flux or very high constant wall temperature with very small vapour quality. A vapour film forms at the wall that separates the liquid from the wall. Due to high thermal resistance of the vapour film, the wall heat flux drops and the critical heat flux is reached. In dryout boiling crisis, once the critical heat flux is reached, the liquid film disappears at the wall, which then becomes covered with vapour. In dryout the critical heat flux drops sharply with the quality. Dryout boiling occurs at high vapour quality.

1.2 Literature Review

Coupled map lattice (CML) has been recognized as a powerful tool of analysis to grasp the qualitative and fundamental nature of complex boiling phenomena and has been applied to many physical systems (Yanagita and Kaneko, 1993). The CML method is based on a dynamic system with continuous field variables but discrete space and time, in which local dynamics propagates in space by diffusion or flow and time is advanced by repeated mapping.

From the study of non-linear chaos dynamics it is known that a complex physical system is not always governed by a complex system of equations. Earlier studies of boiling based on non-linear dynamics, though few and recent, suggest that boiling is a kind of spatio-temporal chaotic phenomenon. The relevant papers in this regard are by Sadasivan et al. (1995), Shoji and Tajima (1997), Shoji (1998), Ellepola and Kenning (1996) and Nelson et al. (1996). However, applications to CML are not restricted to the problems in spatio-temporal chaos, but include pattern formations, some solid-state problems, biological information processing and engineering problems (Kaneko, 1993).

Using the CML method, Yanagita (1992) simulated the pool boiling phenomenon and succeeded in explaining the mode of transition from nucleate to film boiling. He assumed that fundamental dynamic processes of boiling are thermal convection, bubble rising motion and phase change. Although Yanagita's model is very attractive and path breaking, it deviates from actual boiling process at some points. Firstly, his model permits liquid to evaporate in the bulk, a phenomenon known as homogeneous nucleation, which is different from boiling in the usual sense. Secondly, in Yanagita's model, pool boiling takes place even when the heater surface temperature is less than the saturation temperature of the liquid. This never happens in the actual boiling systems. Finally, the strict mode of film boiling is not realized by Yanagita's model.

Shoji (1998) corrected the deficiencies of the model of Yanagita by including nucleation sites on the heater surface and the Taylor instability. The model was applied to saturated and transient pool boiling of water on a small heated surface at 1 atmospheric pressure. The effects of liquid subcooling and surface roughness were also investigated. Although Shoji's model is basically sound, it has the following limitations. Firstly, the calculation of nucleation superheat distribution is sketchy and

cannot be easily reproduced by other researchers. Secondly, no effect due to stirring action of bubbles is incorporated into his model. Finally, rather than using actual heat flux he used an apparent heat flux (without a unit) to plot the pool boiling curve and hence no information about the predicted CHF could be obtained.

Ghoshdastidar et al. (2004) modified the basic theoretical model proposed by Shoji (1998) in terms of nucleation superheat distribution and mixing. The stirring action of the bubbles was modelled by increasing the fluid thermal diffusivity by an enhancement factor. The effectiveness of the enhancement factor approach in the model of Ghoshdastidar et al. (2004) is clearly seen in its capability of reproducing the saturated pool boiling curve well and predicting the critical heat flux (CHF) in the same order of magnitude of the actual value.

So far no studies showing CML simulation of flow boiling have been found in the open literature. The present work is a first attempt in this direction. In this work non-stratified flow boiling of water as well as propane in a horizontal tube whose wall is maintained at constant temperature which is greater than the saturation temperature of the liquid at the entrance pressure is simulated by CML. The liquid is entering the tube in a sub-cooled condition.

1.4 Objectives

The objectives of present work are:

(a) To develop a clear-cut methodology of producing a nucleation superheat distribution on the heated surface.

(b) To find out the axial velocity distribution and mean velocity of the fluid at any circular cross section of the tube.

(c) To find out temperature distribution and mean temperature of the fluid at any circular cross section of the tube.

(d) To find out the mean heat transfer coefficient, mean heat flux and vapour fraction as a function of the axial coordinate.

(e) To include the effect of stirring action of the bubbles.

(f) To carry out a parametric study, for various levels of entry sub-cooling, wall temperatures and mass flow rates.

(g) To find out the axial coordinate beyond which critical heat flux might occur.

Note: T_{sat} corresponds to $p_{entrance}$

T_w ($>T_{sat}$)

T_{in}

($<T_{sat}$)

Liquid

r

r_o

D

z

L

r

θ
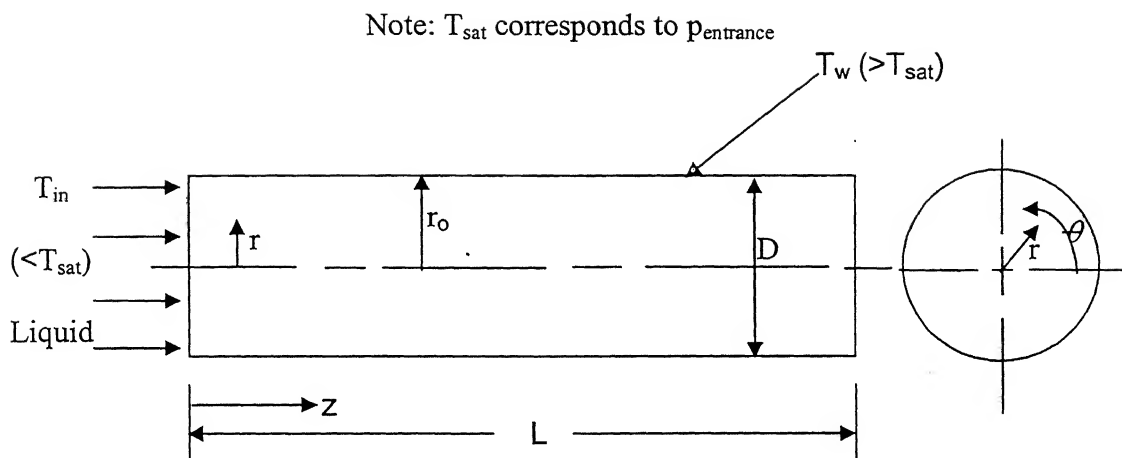
Fig. 1.1 The flow geometry and the computational domain

WALL AND FLUID TEMP VARIATION

Fluid temp

Wall temp

$x=1$

Vapour core temp

Fluid temp

Wall temp

Liquid core temp
$x=0$

Fluid temp

Sat temp

'Dryout'

FLOW PATTERNS

Single-phase vapour

Drop flow

Annular flow with entrainment

Annular flow

Slug flow

Bubbly flow

Single-phase liquid

HEAT TRANSFER REGIONS

Convective heat transfer to vapour

Liquid deficient region

Forced convective heat transfer thro' liquid film

Saturated nucleate boiling

Subcooled boiling

Convective heat transfer to liquid

H
G
F
E
D
C
B
A

Fig.1.2 Various regimes of flow boiling in a vertical heated tube (Collier, 1972)
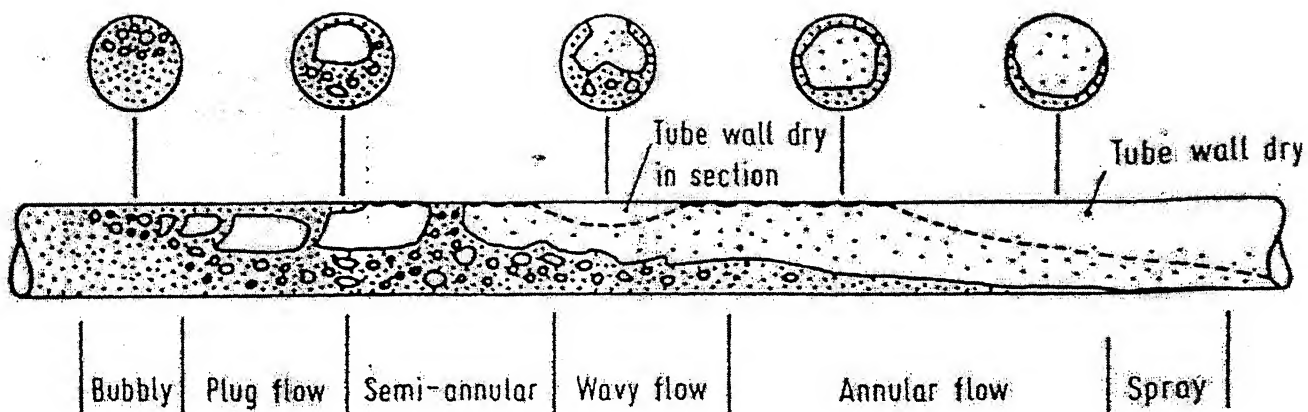
Fig 1.3 Various regimes of flow boiling in a heated horizontal tube for a non-stratified flow (Stephan, 1992)

CHAPTER 2

PROBLEM FORMULATION

2.1 Modeling

In this chapter the problem formulation for the flow boiling of water is described but the general procedure is applicable to other fluids as well. Flow boiling of water at high pressure in a circular horizontal cylindrical tube is considered. The flow is assumed to be hydrodynamically fully developed but thermally undeveloped.

In this work flow boiling is investigated in horizontal tube of diameter .02 m and length 9m. The temperature distribution in the tube wall is ignored as it has a very high thermal conductivity and small thickness. The three dimensional boiling field is approximated and modeling is based on CML. No prior assumption regarding the chaotic nature of the boiling phenomena needs to be made.

2.2 Computational domain and lattices

The computational domain in the r - θ plane is divided into 20×20 lattices as shown in Fig. 2.1. Each lattice can contain either liquid or vapor. There are 20 grid points in the radial direction, 20 grid points in the angular direction and 10 grid points in the axial direction. The dots in Fig. 2.1 represent grid points. The broken lines in the same Figure indicate the faces of lattices. Each lattice contains one grid point at its center. A typical lattice is shown by the shaded region in Fig. 2.1. Grid points at the boundary are surrounded by half–lattices, as shown in Fig. 2.1. A grid point is designated by (i, j, k) with 'i' increasing in the radial (r) direction, 'j' in the angular (θ) direction and k in axial (z) direction. A lattice that encloses a grid point (i, j, k) is also referred to as (i, j, k).
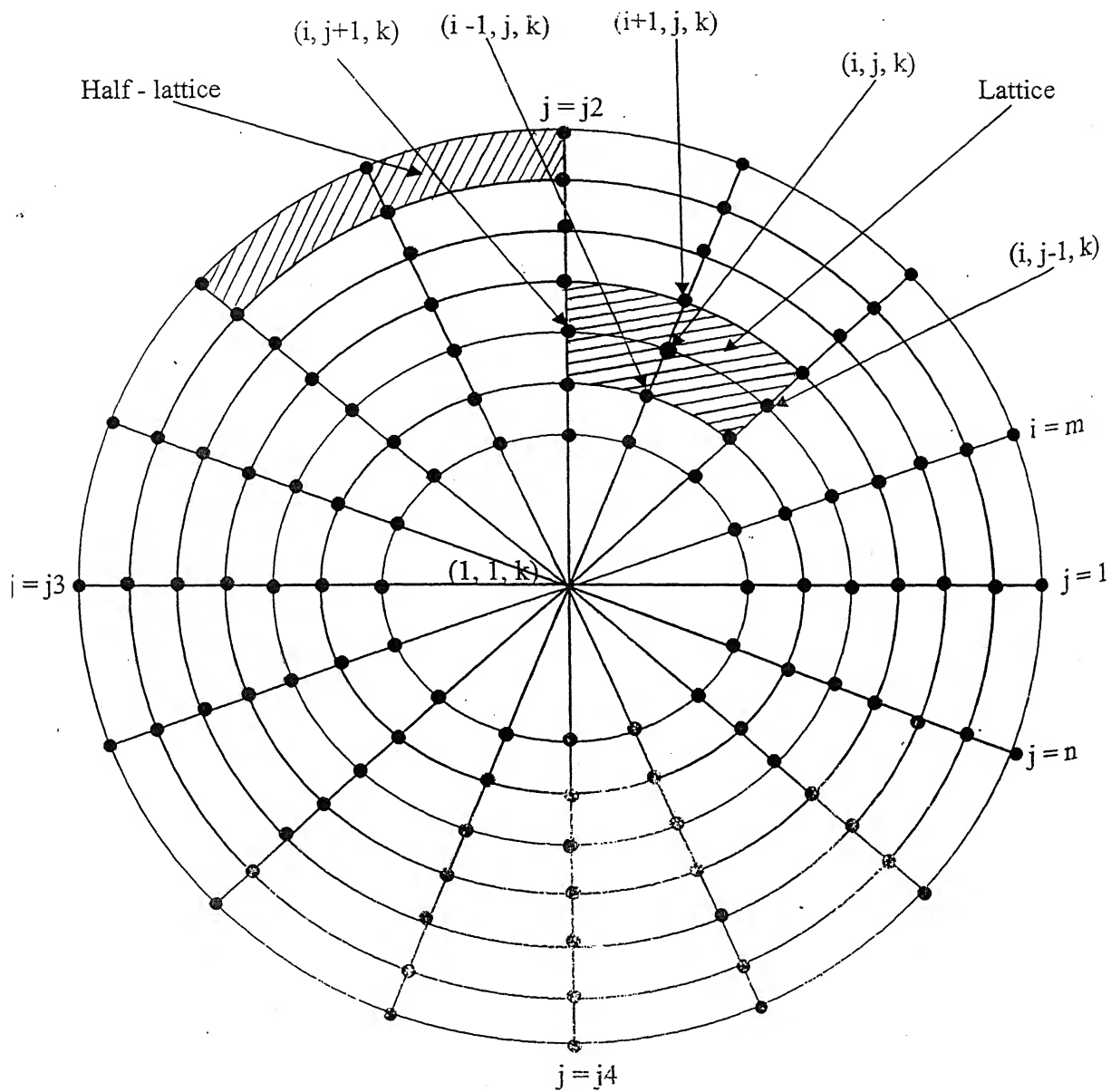
Fig. 2.1 Grid in (r, θ) plane and pictorial representation of the treatment of the condition

2.3 Field variable

For simplicity, temperature is employed as the only one field variable. In addition, a flag function, $F_{i, j, k}$ is used for the convenience of calculations to show the phase of each lattice. $F_{i, j, k}$ = '0' and '1' represent the lattice (i, j, k) in liquid and vapor phases respectively.

2.4 Formulation of dynamic process

In the CML method, dynamic processes are usually formulated in mappings. In the present model, it is assumed that boiling is governed by the following physics and dynamics.

2.4.1 Nucleation on the heated surface

According to Wang and Dhir (1993), nucleation cavities are distributed at random on the heated surface. Many cavities are distributed on each surface lattice but if it is assumed that every cavity has a conical shape, a larger cavity yields lower nucleation superheat. Therefore, only the cavity of maximum size [in this case, D_c as calculated from equation (2.2)] is employed, since the active cavity of each surface lattice which determines the local nucleation superheat, ΔT_{act} [equation (2.1)], is required for bubble nucleation. The term βR is added to D_m to create a randomness among the size of the large cavities. The nucleation superheat is given by

$$\Delta T_{act} = T_{act} - T_{sat} = \frac{4\sigma T_{sat}}{\rho_v h_{fg} D_c} \tag{2.1}$$
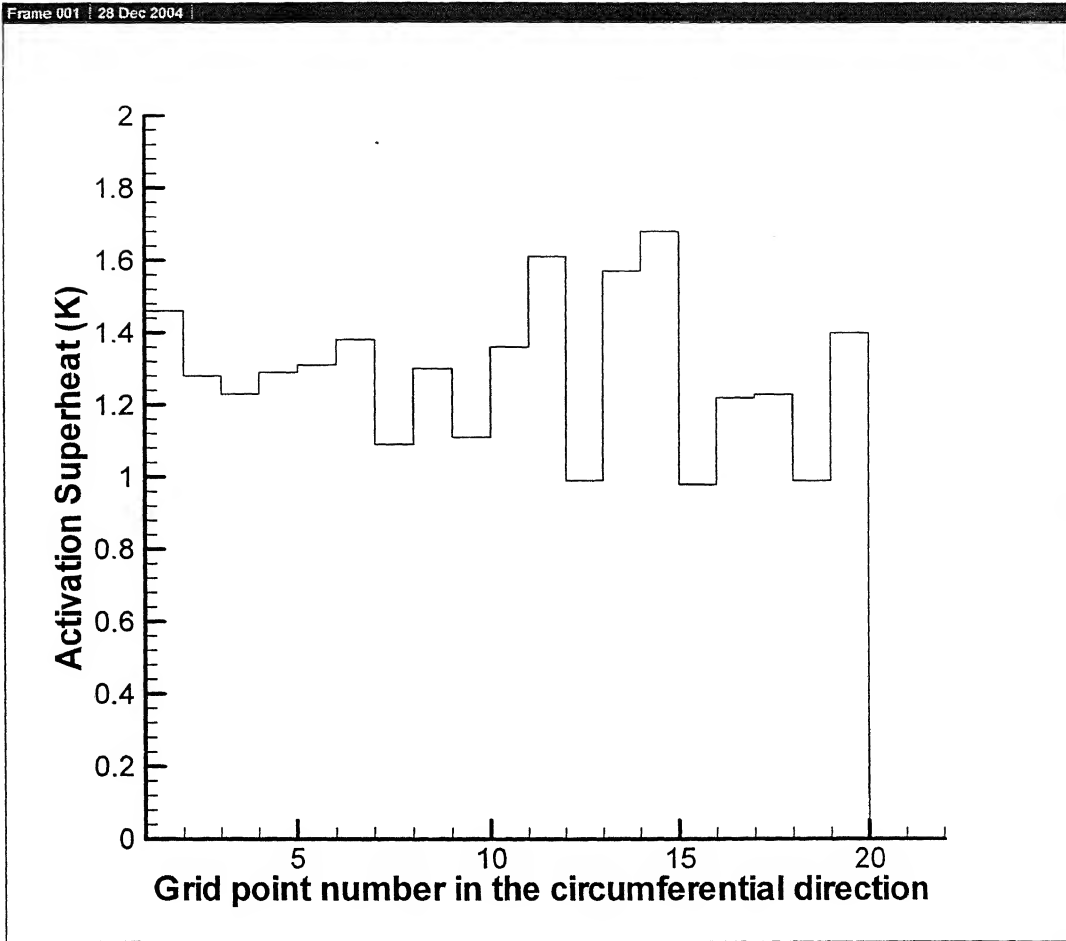
Fig. 2.2 Circumferential Nucleation Superheat Distribution for Water at the tube
entrance

Where D_c is the diameter of the largest nucleation cavity on a surface lattice. To calculate D_c, the following formula is used:

$$D_c (m, j, k) = D_m + \beta R \qquad (2.2)$$

Where $D_c (m, j, k)$ represents the diameter of the largest nucleating cavity on the lattice (m, j, k), D_m is the minimum diameter of nucleating cavities on a heater surface lattice, β, which is assigned a value of 0.99, indicates the maximum deviation from D_m and has same unit as D_c and D_m, i.e. micrometer, and R is a random number between 0 and 1 assigned at the jth surface lattice. Although the number of grid points in the circumferential direction is taken as 20 in the present study, it may be varied. A total of 1020 random numbers is generated using a NAG library random number generator

subroutine. Every 50th random number of the set is employed at each surface lattice starting from the first.

The minimum cavity diameter is arbitrarily taken as 1 μm. It is assumed that sites smaller than 1 μm do not exist on this particular heater surface. Thus, the maximum diameter of the nucleating cavities on a heater surface lattice becomes 1.99 μm as calculated from equation (2.2) when the random number takes on a value of 1.

Thus, using equations (2.1) and (2.2), the nucleation superheat distribution on the heated surface is calculated. Fig 2.2 shows a typical distribution of nucleation superheat at a particular axial location.

2.4.1.1 Nucleation Modelling

Case I: (Nucleation not suppressed)

If at a particular axial location (k)

$T_{sat (k)}$ - $T_{mean (k)}$ > 0, and if $T_{(m, j, k)}$ > $T_{act (j, k)}$, where j = 1 to n

and $F_{(i, j, k)}$ = 0, where i = 1 to m , j = 1 to n

then $F_{(i, j, k)}$ = 1, where i = 18, j = 1 to n $\hspace{2cm}$ (2.3)

if T_{sat} - T_{mean} > 15 ^{0}C.

if T_{sat} − T_{mean} < 15 ^{0}C, then i = 10 in equation (2.3)

Case II: (Suppression of Nucleation)

If at a particular axial location (k)

$T_{sat (k)}$ − $T_{mean (k)}$ < 0, and if $T_{(m, j, k)}$ > Tact (j, k) and if $F_{(i, j, k)}$ = 0, where i = 1 to m, j = 1 to n,

then F (m, j, k) = 1, where j = j3 to n $\hspace{2cm}$ (2.4)

and F (i, j, k) = 1, where j = 1 to j3, i = 2 $\hspace{2cm}$ (2.5)

To sum up the procedure of obtaining the nucleation superheat distribution, the following points should be kept in mind. The most important point in the calculation of nucleation superheat distribution is the minimum cavity diameter, D_m, on a surface lattice. It may be noted that the minimum cavity diameter is assumed to be the same for all surface lattices in the present problem. If, for a given surface, D_m is provided then the nucleation superheat distribution can be calculated by the combined application of equation (2.2) and equation (2.1). The following needs to be said about the physical (and mathematical) basis of equation (2.2). Since β is the maximum deviation from the minimum cavity

diameter, the product of β and the random number R, which takes a value between 0 and 1, essentially implies that a fraction of that maximum deviation is taken. The product [i.e. βR] is then added to the minimum value, D_m, to get D_c from equation (2.2). It can be easily seen that D_c can vary from 1 to 1.99 μm. The deviation β does not have to have fixed value. The choice of a value for β should be dictated by the information the analyst has about the minimum cavity size on a given surface lattice and the maximum cavity size on the heater surface. Thus, β may vary from one surface to other.

2.4.2 Governing Equations:

Assuming the flow to be laminar and fully developed ($v_r = 0$, $\dfrac{\partial v_z}{\partial z} = 0$) and having no swirl ($v_\theta = 0$), the z- momentum equation takes the form

$$\rho \frac{\partial v_z}{\partial t} = -\frac{\partial p}{\partial z} + \mu \frac{1}{r}\frac{\partial}{\partial r}(r\frac{\partial v_z}{\partial r}) + \mu \frac{1}{r^2}\frac{\partial^2 v_z}{\partial \theta^2} \qquad (2.6)$$

In the above equation, $\dfrac{\partial p}{\partial z}$ is assumed to be a known quantity with p decreasing linearly with z.

At t = 0, $v_z = 0$ $\qquad\qquad\qquad\qquad\qquad\qquad\qquad\qquad\qquad$ (2.7)

At r = 0, v_z = finite $\qquad\qquad\qquad\qquad\qquad\qquad\qquad\qquad$ (2.8)

At $r = r_0$, $v_z = 0$ (no slip) $\qquad\qquad\qquad\qquad\qquad\qquad$ (2.9)

In addition the following periodic boundary conditions are valid.

$$\mu \frac{1}{r}\frac{\partial v_z}{\partial \theta}\bigg|_{r,\theta} = \mu \frac{1}{r}\frac{\partial v_z}{\partial \theta}\bigg|_{r,\theta+2\pi} \qquad (2.10)$$

$$(v_z)\big|_{r,\theta} = (v_z)\big|_{r,\theta+2\pi} \qquad (2.11)$$

The equation is:

$$\rho c_p \frac{\partial T}{\partial t} + \rho c_p v_z \frac{\partial T}{\partial z} = k_f\left[\frac{1}{r}\frac{\partial}{\partial r}(r\frac{\partial T}{\partial r})\right] + \frac{k_f}{r^2}\frac{\partial^2 T}{\partial \theta^2} \qquad (2.12)$$

At t = 0, $T = T_{sat} - \Delta T_{sub}$ $\qquad\qquad\qquad\qquad\qquad\qquad$ (2.13)

At z = 0, $T = T_{sat} - \Delta T_{sub}$ $\qquad\qquad\qquad\qquad\qquad\qquad$ (2.14)

At r = 0, T = finite $\qquad\qquad\qquad\qquad\qquad\qquad\qquad\qquad$ (2.15)

At $r = r_0$, $T = T_w$ ($T_w > T_{sat}$) $\qquad\qquad\qquad\qquad\qquad$ (2.16)

Also, the following periodic boundary conditions apply.

$$-\frac{k_f}{r}\frac{\partial T}{\partial \theta}\bigg|_{r,\theta} = -\frac{k_f}{r}\frac{\partial T}{\partial \theta}\bigg|_{r,\theta+2\pi} \tag{2.17}$$

$$T\bigg|_{r,\theta} = T\bigg|_{r,\theta+2\pi} \tag{2.18}$$

The momentum and energy equations are solved by the explicit finite – difference method (see Appendix A). $\Delta z = 1m$, $\Delta r = 5.26 \times 10^{-4}$ m, $\Delta \theta = 18^0 = .35415$ rad. $\Delta t = 10^{-5}$ s is used to cause stability.

2.4.3 Accuracy:

The solution has been validated with the analytical solutions for single phase flow and heat transfer (the fluid is water). Some representative plots are shown in Figure nos. 2.3, 2.4 and 2.5. In Fig. 2.4 Nusselt number clearly approaches the steady state analytical solution, that is, 3.66 with increasing time. The analytical solution in Fig. 2.2 has been obtained from Bird et al. (1960). The analytical solution in Fig. 2.3 has been taken from Fox and McDonald (1995).

2.4.4 Phase change and effects of bubble motion:

It is known that latent heat is consumed when liquid evaporates and is released when vapor condenses. This phase change process is formulated as follows (Shoji, 1998):

$$\text{If } F_{i,j,k} = 0 \text{ and } T_{i,j,k}^{p} > T_{c(i,j,k)} \text{ then } T_{\eta(i,j,k)}^{p} = T_{\eta(i,j,k)}^{p} - \eta \tag{2.19}$$

$$\text{If } F_{i,j,k} = 1.0 \text{ and } T_{i,j,k}^{p} < T_{c(i,j,k)} \text{ then } T_{\eta(i,j,k)}^{p} = T_{\eta(i,j,k)}^{p} + \eta \tag{2.20}$$

The suffix $\eta(i, j, k)$ represents the nearest neighboring four lattices and $T_{c(i,j,k)}$ is the phase change temperature, which is determined according to the phase change criteria given below. In equations (2.19) and (2.20), η is a parameter related to the enthalpy of vaporization and has a unit of ^{0}C. The aforesaid equations also represent the mixing effect of bulk liquid due to bubble motion.

2.4.4.1 Phase change criteria

The value of $T_{c\,(i,\,j,\,k)}$ for the liquid lattice adjacent to the wall is nucleation superheat, as shown in Fig.2.2. The value for liquid lattices in the bulk is assumed to be the homogeneous nucleation temperature of the liquid, but for liquid lattice neighboring the vapor lattice, is the saturation temperature of the liquid.

15
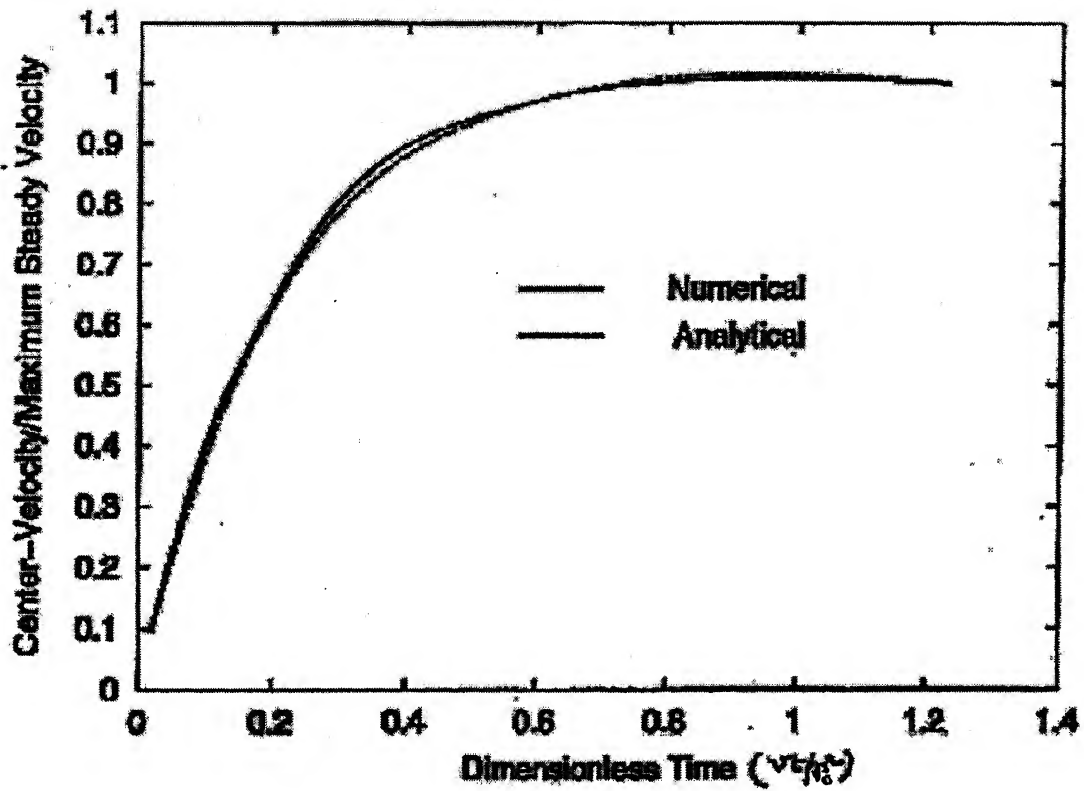
Fig. 2.3 Unsteady state centre velocity in pipe flow
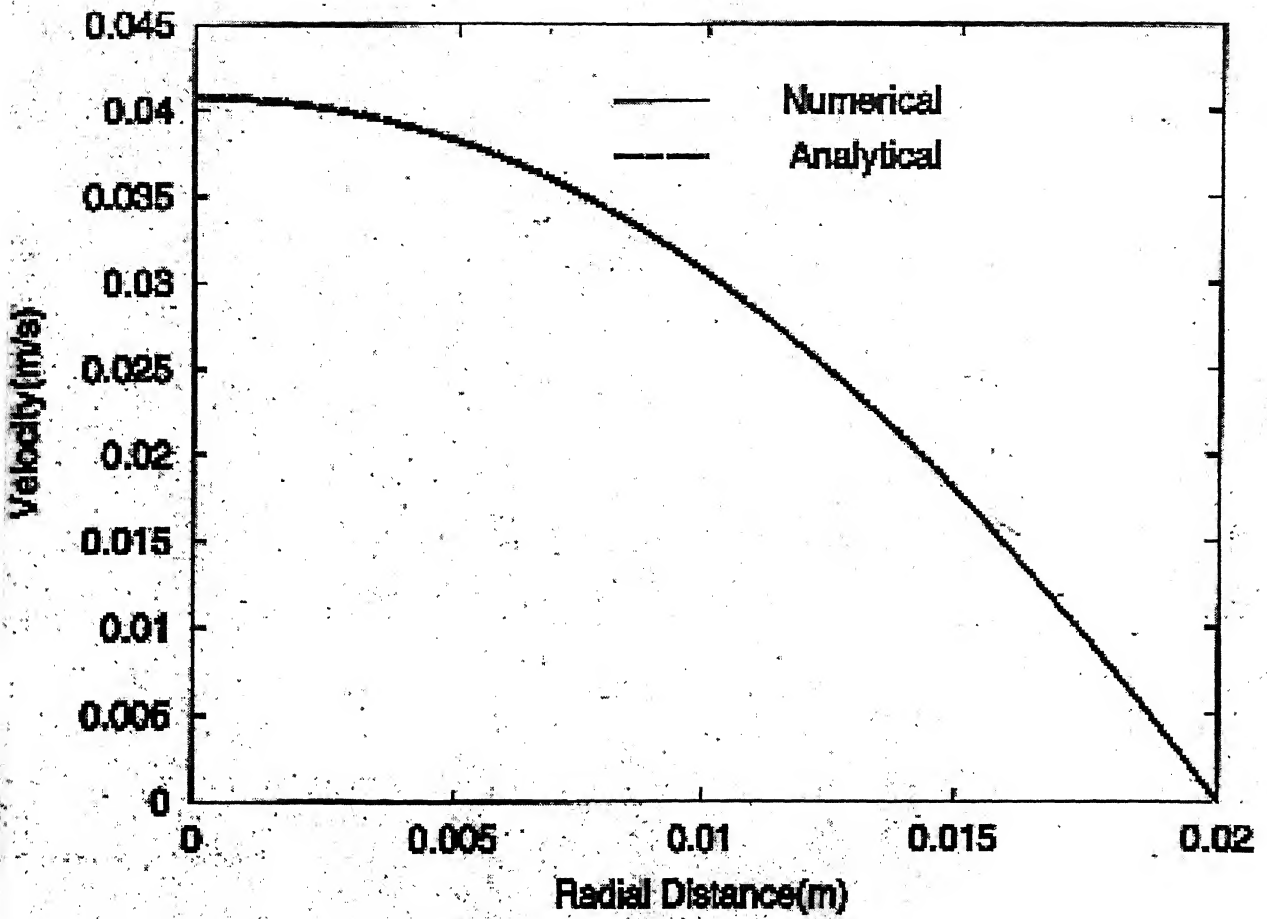
Fig. 2.4 Fully developed steady laminar velocity profile in a pipe
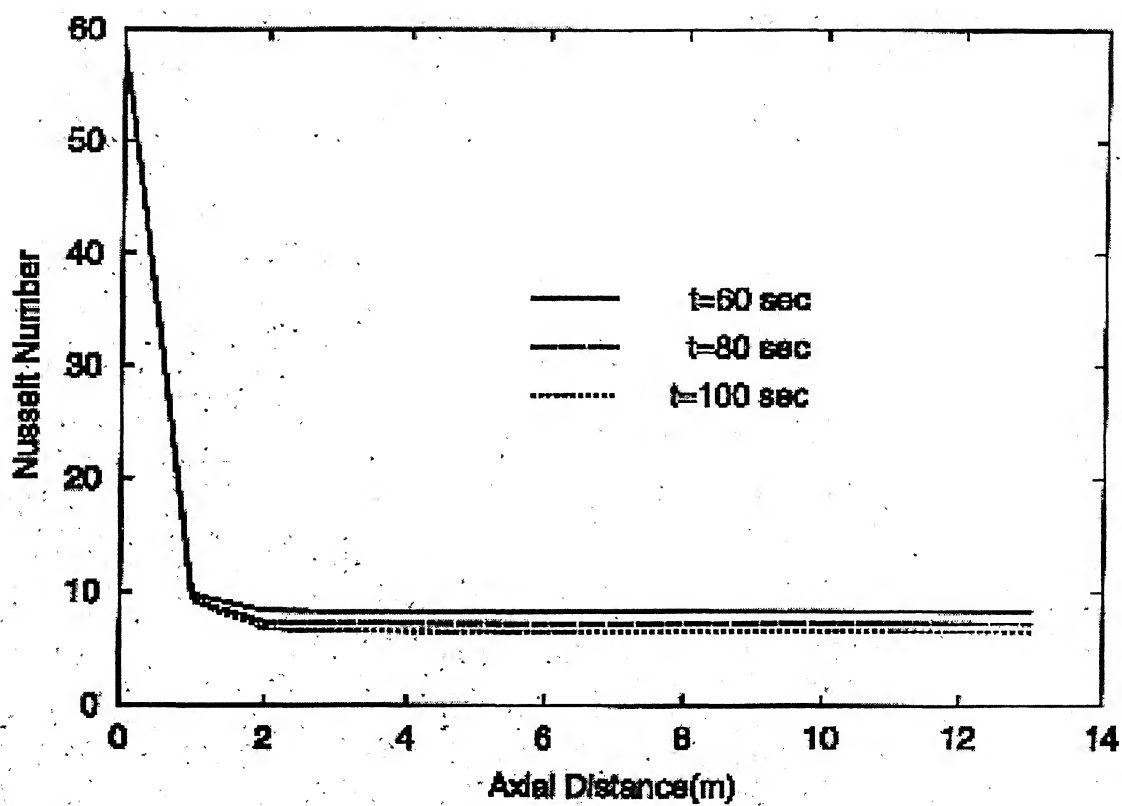
Fig 2.5 Transient Nusselt Number profile in a pipe flow

CHAPTER 3

METHOD OF SOLUTION

3.1 Solution methodology

In this chapter the method of solution by CML and overall solution algorithm is presented.

3.1.1 Time advancement

Time is advanced by repeating a set of mapping the dynamic processes (Section 2.4.2 to 2.4.4) in such a manner that

$$T^p \rightarrow T' \rightarrow T^{p+1} \tag{3.1}$$

Where the superscripts p and p+1 indicate the present and future time values of the temperature.

3.1.2 Parameter values

In the CML method, the parameter values are determined so as to reproduce the phenomena satisfactorily. In the present computations, the parameter value is

$\eta = .01$

3.1.3 Overall solution algorithm

1. Specify wall temperature $T_{wall} = 230^0C$.

2. Calculate fluid properties with pressure, as the pressure changes along the axial direction, due to pressure drop.

3. Initialize temperature T, and velocity v_z.

4. Calculate v'_z by solving momentum equation [equation (2.6)].

5. Check Reynolds number. If Reynolds number exceeds 2000, then respecify $\frac{\partial p}{\partial z}$.

6. Calculate T' by solving the energy equation [equation (2.12)].

7. Apply the nucleation criteria [equations (2.3), (2.4), (2.5)].

8. Determine the phase state of each fluid lattice by using phase change criteria.

9. Apply equations (2.19) and (2.20) to obtain T^{p+1}.

10. Check the phase state of each fluid lattice again.

11. Is steady state reached? If yes, go to step 13. If not calculate the overall vapour fraction, f (by volume), and equivalent density, specific heat and thermal conductivity and diffusivity, viscosity and kinematic viscosity of the liquid/vapour mixture using the following equations, enhance the molecular thermal conductivity and diffusivity, viscosity and kinematic viscosity of the fluid by a suitable factor as described below to include the effect of mixing effect of the bubbles and go to step 4:

$k_{eq} = f k_v + (1-f) k_l$

$\rho_{eq} = f \rho_v + (1-f) \rho_l$

$c_{eq} = f c_v + (1-f) c_l$

$\mu_{eq} = f\mu_v + (1-f)\mu_l$

The overall vapour fraction, f, is defined as the ratio of the volume of vapor and the volume of (liquid + vapour) mixture in the pool.

For all values of f, the enhancement factor is 1.2.

The enhancement factor basically takes into account the turbulent mixing in the   fluid resulting from the bubble stirring action which enhances the thermal diffusivity, kinematic viscosity of the fluid.

12. Calculate the steady state average nusselt number, average heat transfer coefficient a any circular cross section of the tube.

13. From 13, calculate steady state wall heat flux.

$q^{//}(k) = h_{mean}(k)(T_{wall} - T_{mean}(k))$, where k = 1 to 9.

14. Print the axial location, heat flux, heat transfer coefficient, vapour fraction.

15. STOP

A concise flowchart of the solution algorithm is shown in Fig. 3.1

```
                        ╭─────────────╮
                        │    START    │
                        ╰─────────────╯
                               │
                               ▼
              ╱────────────────────────────╲
             ╱  INPUTDATA, T_wall             ╲
            ╱   =230^0c, T^P                    ╲
           ╱────────────────────────────────────╲
                               │
                               ▼
                       ┌───────────────┐
                       │  t = Δt        │
                       │  ITER =0       │
                       └───────────────┘
                               │
                               ▼
                    ┌────────────────────┐
   ┌────────────────▶│   MOMENTUM         │   V_z^{/}
   │                 │   EQUATION         │
   │                 └────────────────────┘
   │                          │
   │                          ▼
   │                 ┌────────────────────┐
   │                 │   ENERGY           │   T^{/}        ┌──────────────┐
   │                 │   EQUATION         │◀───────────────│  NUCLEATION  │
   │                 └────────────────────┘                └──────────────┘
   │                          │
   │                          ▼
┌───────────────┐   ┌────────────────────┐
│ t = t + Δt     │   │  PHASE CHANGE      │   T^{p+1}
│ ITER=ITER+1    │   │  AND MIXING        │
└───────────────┘   └────────────────────┘
   ▲                          │
   │                          ▼
┌───────────────┐        ╱─────────────────╲
│ FIND THE      │       ╱                   ╲
│ EQUIVALENT    │      ╱   IS STEADY STATE   ╲
│ PROPERTIES    │  NO ╱    REACHED?           ╲
│ AND INCREASE  │◀───《                        》
│ THE           │     ╲                       ╱
│ DIFFUSIVITY   │      ╲                     ╱
│ BY  AN        │       ╲                   ╱
│ ENHANCEMENT   │        ╲─────────────────╱
│ FACTOR        │                 │ YES
└───────────────┘                 ▼
              ┌──────────────────────────────────────────────────────┐
              │ PRINT AXIAL LOCATION, HEAT FLUX, HT-COEFF, VAP-FRAC    │
              └──────────────────────────────────────────────────────┘
                               │
                               ▼
                        ╭─────────────╮
                        │    STOP     │
                        ╰─────────────╯
```
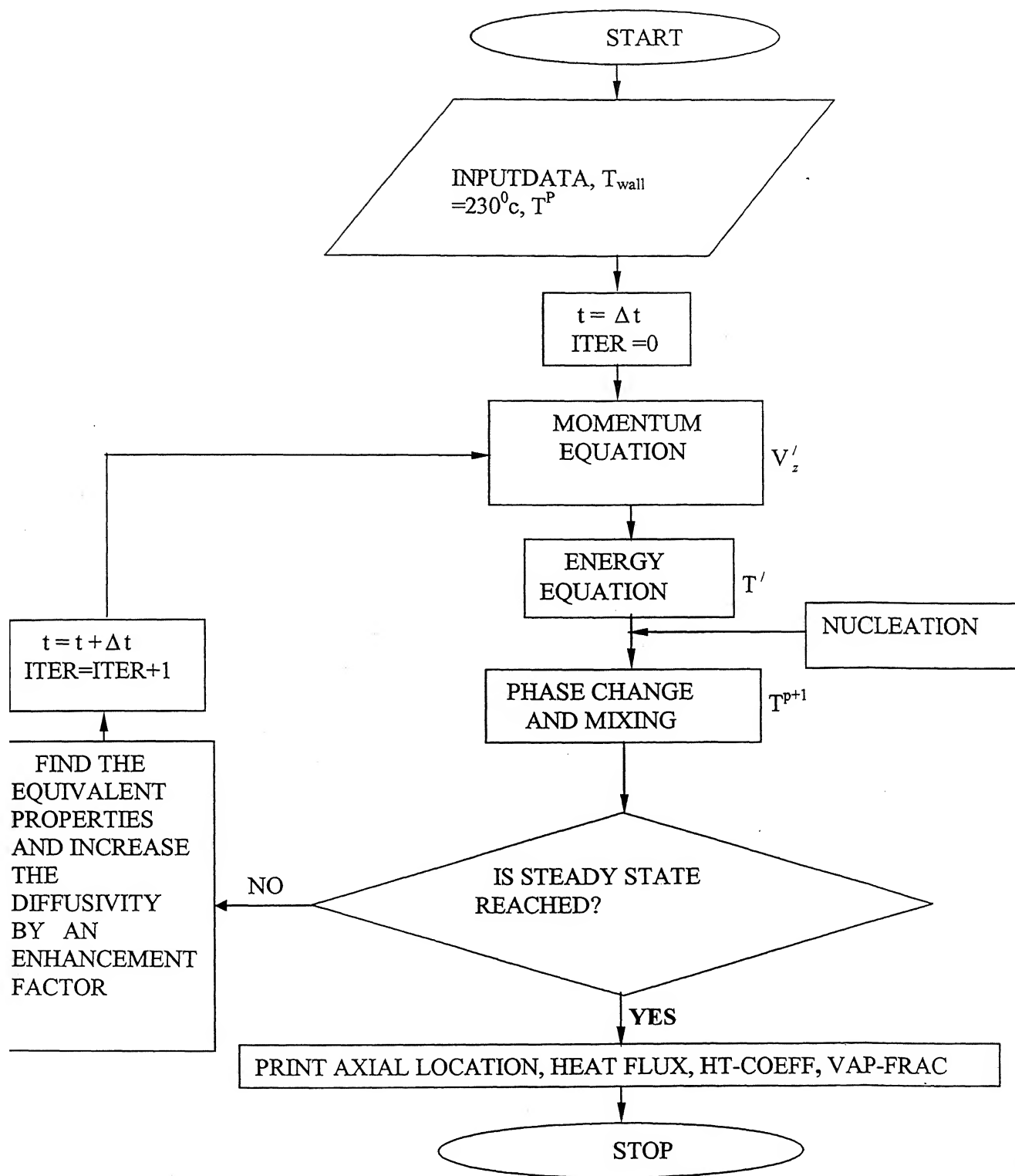
Fig 3.1 Flow chart of the overall solution algorithm

CHAPTER 4

RESULTS AND DISCUSSION

4.1 Introductory Remarks

This chapter presents a parametric study of heat transfer coefficient, heat flux, fluid mean temperature and vapour fraction versus axial coordinate of the horizontal tube for various levels of entry subcooling, wall temperatures and mass flow rates. It may be noted that pressure changes along the axis and as a result the saturation temperature (T_{sat}) and thermophysical properties of the liquid and vapour also vary. T_{sat} and property variations with respect to pressure have been represented in the form of equations for convenience in computer implementation. These relations can be found in Appendix B for water as well as propane. The results shown here correspond to t = 1 sec. Note that $\Delta t = 10^{-5}$ s is used. Because of CPU time limitation, the results for higher time and steady state could not be obtained. The heat transfer coefficient actually is the mean value. It is defined as follows.

$$h_{mean}(z) = \frac{\dfrac{1}{2\pi}\displaystyle\int_0^{2\pi} q_r''(\theta,z)d\theta}{T_w - T_{mean}(z)} = \frac{q''(z)}{T_w - T_{mean}(z)} \tag{4.1}$$

The heat flux is defined as

$$q''(z) = \frac{1}{2\pi}\int_0^{2\pi} -k_f \left.\frac{\partial T}{\partial r}\right|_{r=r_0} d\theta \tag{4.2}$$

The fluid mean temperature is basically the mixed mean temperature or mixing – cup temperature.

$$T_{mean} = \frac{1}{A v_{mean}}\int_A v_z T dA = \frac{1}{\pi r_0^2 v_{mean}}\int_0^{2\pi}\int_0^{r_0} v_z(r,\theta)T(r,\theta)drd\theta \tag{4.3}$$

Where,

$$v_{mean} = \frac{1}{A}\int_A v_z dA = \frac{1}{\pi r_0^2}\int_0^{2\pi}\int_0^{r_0} v_z(r,\theta)drd\theta \tag{4.4}$$

The vapour fraction (f) is actually the volume fraction or void fraction which is defined as the ratio of the cross – sectional area (A_v) filled by the vapour at any location along the tube length to the total cross – sectional area (A) of the tube. Thus,

$$f = \frac{A_V}{A}$$ (4.5)

These fractions do not change within a sufficiently small tube section Δz. Thus,

$$f = \frac{A_V \Delta z}{A \Delta z}$$ (4.6)

Therefore, the volume fraction (which is the same as the void fraction) of the vapour in the tube section under consideration is then

$$f = \frac{V_V}{V}$$ (4.7)

4.2 Flow boiling of water

4.2.1 h_{mean}, q'', T_{mean}, f vs. z for $T_{wall} = 230^0C$, $\Delta T_{sub} = 30^0C$, $p_{entrance} = 25$ bar

Figs 4.1 – 4.4 show h_{mean} vs. z , q'' vs. z, T_{mean} vs. z and f vs. z respectively for flow boiling of water when $\frac{\partial p}{\partial z} = -1.5 N/m^3$, $T_{wall} = 230^0C$ and $T_{entrance} = T_{sat\ at\ p\ entrance} - \Delta T_{sub}$ where $\Delta T_{sub} = 30^0C$. Fig. 4.1 shows that there is a steep drop of h_{mean} near the entrance because of high T_w - T_{sat}. At z = 4m there is again a drop of heat transfer coefficient. This can be explained by the sudden rise of vapour fraction at that location as indicated in Fig. 4.4 and hence the conductivity of the liquid – vapour decreases because of higher vapour content. Thus the critical heat flux corresponding to z = 4m is around 2000 W/m^2 as revealed in Fig. 4.2. Hence, z = 4 m may be considered as the length beyond which the tube runs the risk of getting irreversibly damaged. Fig. 4.3 indicates initial steep rise of mean temperature of the fluid followed by almost constant temperature region up to z = 4 m. After this zone there is a drop in the mean temperature because of a drop in the heat transfer coefficient as revealed in Fig. 4.1. T_{mean} then further drops a little but shows a slight rise towards the end. This is because towards the exit of the tube vapour fraction is high and so is the vapour velocity resulting in more or less constant heat transfer coefficient as the effect of low vapour conductivity is compensated by high vapour velocity.

23

4.2.2 Parametric Study

4.2.2.1 h_{mean}, q'', T_{mean}, f vs. z for different wall temperatures for $\Delta T_{sub} = 30^0C$, $\frac{\partial p}{\partial z} = -1.5$ N/m^2.

Fig. 4.5 shows that wall temperature has no effect on the heat transfer coefficient. Fig. 4.6 reveals that heat flux increases with wall temperature as $T_w - T_{sat}$ is high. As expected greater wall temperature results in greater levels of mean fluid temperature as depicted in Fig. 4.7. Interestingly, increasing the wall temperature from 230^0C to 300^0C does not change the vapour fraction (Fig. 4.8). This clearly shows that h_{mean} is a function of vapour fraction.

4.2.2.2 h_{mean}, q'', T_{mean}, f vs. z for different ΔT_{sub}'s for $T_{wall} = 230^0C$ and $\frac{\partial p}{\partial z} = -1.5$ N/m^3.

Fig. 4.9 shows that with decrease in entry sub-cooling the heat transfer coefficient decreases in the section near the tube entrance but becomes independent of axial location in the latter part of the tube. Heat flux drops with lower levels of entry sub-cooling as revealed in Fig. 4.10, it being the lowest for $\Delta T_{sub} = 0^0C$, that is, when the fluid is entering at saturation condition. Fig. 4.11 shows that fluid mean temperature increases with decreased levels of entry sub-cooling. Fig. 4.11 also shows that as ΔT_{sub} decreases the constant mean temperature zone increases. Fig. 4.12 depicts that near the tube entrance vapour fraction is high for low ΔT_{sub}'s whereas the maximum vapour fraction is same for all ΔT_{sub}'s.

4.2.2.3 h_{mean}, q'', T_{mean}, f vs. z for different mass flow rates for $T_{wall} = 230^0C$, $\Delta T_{sub} = 30^0C$

Fig. 4.13 – 4.16 describe the effect of fluid mass flow rate on variation of h_{mean}, q'', T_{mean} and f respectively along z. The mass flow rate of 0.348×10^{-3} Kg/s corresponds to $\frac{\partial p}{\partial z} = -1.3$ N/m^3, while that of 0.401×10^{-3} Kg/s corresponds to $\frac{\partial p}{\partial z} = -1.5$ N/m^3 and that of 0.482×10^{-3} Kg/s corresponds to $\frac{\partial p}{\partial z} = -1.8$ N/m^3. The results in Fig. 4.13 clearly show that heat transfer coefficient is virtually independent of the mass flow rate in the initial section of the tube where nucleate boiling effect is dominant. On the contrary, in the latter part of the tube convective vapourization is significant. Since

with increased mass flow rates more vapourization occurs in the latter part of the tube (Fig. 4.16), heat transfer coefficient falls due to lower conductivity of vapour. Fig. 4.14 (q'' vs. z) indicates the same trend as in Fig. 4.13. With increased mass flow the drop in the fluid mean temperature occurs at a lower axial location of the tube because of larger vapour formation (Fig. 4.15). Another interesting observation is that at the lowest mass flow rate of 0.348×10^{-3} Kg/s the rise of T_{mean} near the tube exit does not take place. As a matter of fact the mean temperature further falls. This is because the velocity of vapour is not high enough to compensate for the decrease in the vapour conductivity which results in lower heat transfer coefficient.

4.3 Flow Boiling of Propane

This section presents the results for flow boiling of propane. Fig. 4.17 shows a typical circumferential nucleation superheat distribution on the tube wall at the entrance.

4.3.1 h_{mean}, q'', T_{mean}, f vs. z for $T_{wall} = 50^0C$, $\Delta T_{sub} = 10^0C$, $p_{entrance} = 5$ bar

Fig. 4.18 – 4.21 show h_{mean} vs. z, q'' vs. z, T_{mean} vs. z and f vs. z respectively for flow boiling of propane when $\frac{\partial p}{\partial z} = -.3 N / m^3$, $T_{wall} = 50^0C$ and $T_{entrance} = T_{sat\ at\ p\ entrance} - \Delta T_{sub}$

where $\Delta T_{sub} = 30^0C$. The trends are similar to that for water except that the drop in heat transfer coefficient at some location down the tube is not as marked as that for water. Also, in Fig. 4.20 T_{mean} vs. z curve reveals that unlike in water boiling there is no constant temperature zone and there is a much larger latter section of the tube in which increase of temperature is visible.

4.3.2 Parametric study

4.3.2.1 1 h_{mean}, q'', T_{mean}, f vs. z for different wall temperatures for $\Delta T_{sub} = 10^0C$, $\frac{\partial p}{\partial z} = -.3$ N/m^3.

The relevant figures are Figs. 4.22 – 4.25. Here also similar trends are observed as for water. The heat transfer coefficient shows no dependence on wall temperature.

4.3.2.2 h_{mean}, q'', T_{mean}, f vs. z for different ΔT_{sub}'s for $T_{wall} = 40^0C$ and $\frac{\partial p}{\partial z} = -.3$N/m^3.

The relevant figures are Figs. 4.26 – 4.29. The trends similar to water are observed. The exception is Fig. 4.28 where the fluid mean temperature is higher for $\Delta T_{sub} =$

20^0C than for $\Delta T_{sub} = 30^0$C in the section of the tube from $z = 4.8$ m to 6 m, the reason being higher vapour velocity in the former case due to larger vapour content in the convective vapourization zone which is larger than that for $\Delta T_{sub} = 30^0$C.

4.3.2.3 h_{mean}, q'', T_{mean}, f vs. z for different mass flow rates for $T_{wall} = 40^0$C , $\Delta T_{sub} = 10^0$C

Figs. 4.30 – 4.33 describe the effect of fluid mass flow rate on variation of h_{mean}, q'', T_{mean} and f respectively along z. The mass flow rate of 0.292×10^{-4} Kg/s corresponds to $\frac{\partial p}{\partial z} = -.1$ N/m^3, while that of 0.117×10^{-3} Kg/s corresponds to $\frac{\partial p}{\partial z} = -.3$ N/m^3, and that of 0.175×10^{-3} Kg/s corresponds to $\frac{\partial p}{\partial z} = -.6$ N/m^3. The results (Fig. 4.30) show that convective vapourization zone in each section is much larger as compared to the zone where nucleate boiling is dominant. As in the case of boiling of water, heat transfer coefficient is independent of mass flow rate while it decreases with increase in mass flow rate. The trend is same in Fig. 4.31 which depicts q'' vs. z variation. Fig. 4.32 shows that for $\dot{m} = 0.292 \times 10^{-4}$ Kg/s after a steep increase of mean temperature the gradient of temperature in the rest of the tube is constant but much lower than that near the entrance. It is also seen that generally T_{mean} increases for increase in mass flow rate except for one crossing of the temperature curves for $\dot{m} = 0.117 \times 10^{-3}$ Kg/s and $\dot{m} = 0.175 \times 10^{-3}$ Kg/s. Fig. 4.33 reveals that vapour fraction remains constant throughout at a lowest mass flow rate, that is, $\dot{m} = 0.292 \times 10^{-4}$ Kg/s showing very little effect of convective vapourization which for higher mass flow rates the effect of convective vapourization is clearly more visible.
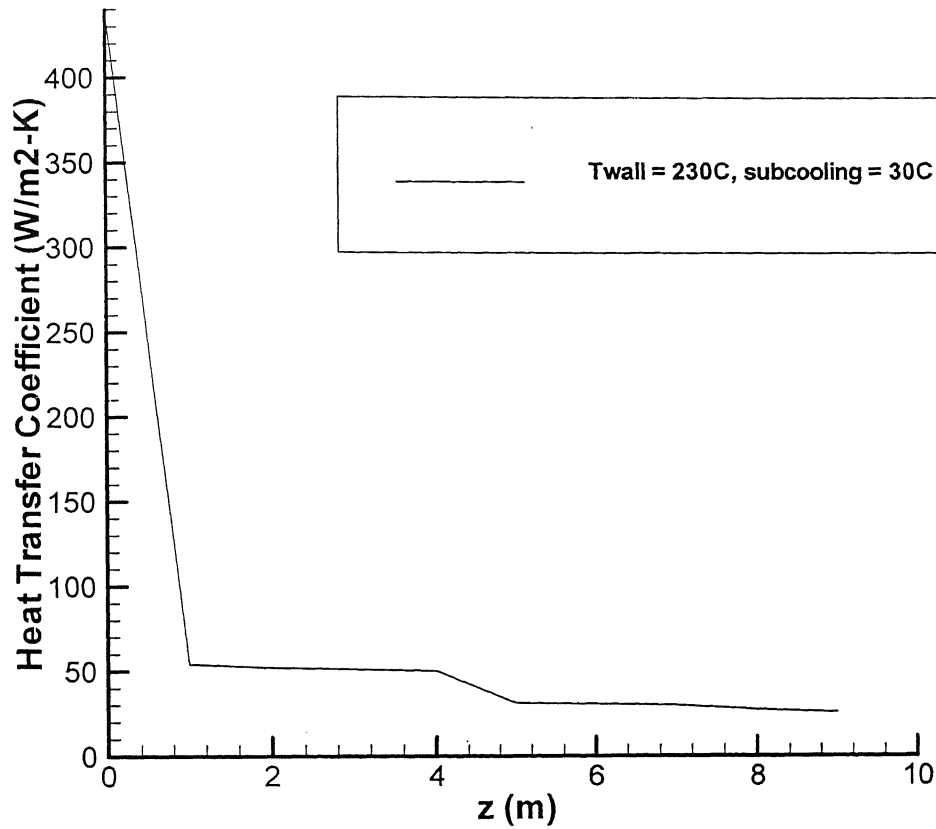
Fig 4.1 Heat Transfer Coefficient versus axial coordinate curve for Water
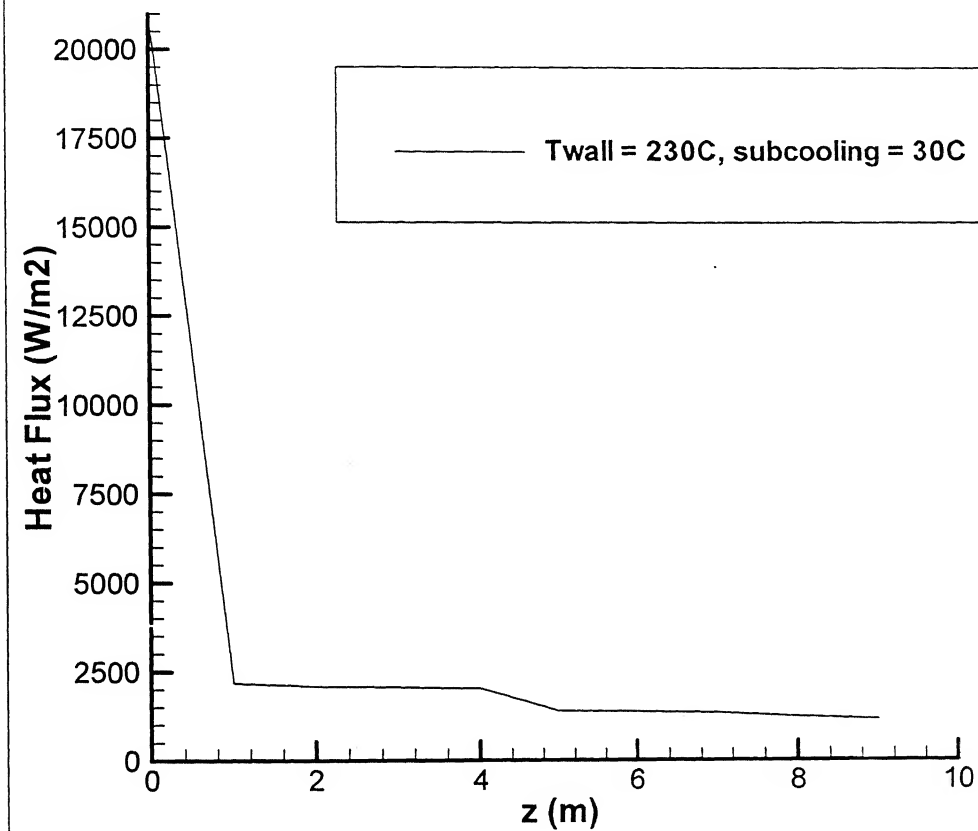
$$\frac{\partial p}{\partial z} = -1.5 \text{ N/m}^3$$

Fig 4.2 Heat Flux versus axial coordinate curve for Water $\dfrac{\partial p}{\partial z} = -1.5 \text{ N/m}^3$
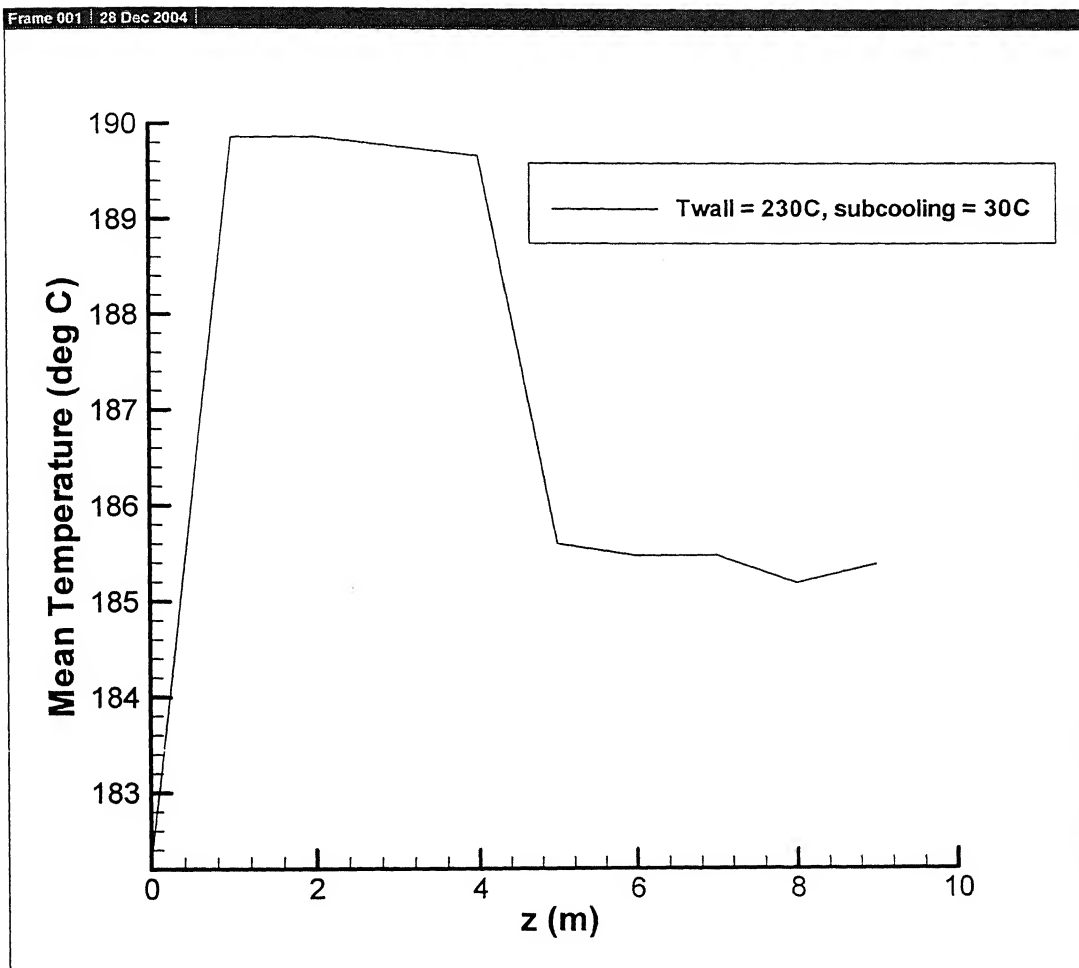
28

Fig. 4.3 Mean temperature of fluid (Tmean) versus axial coordinate curve for Water $\dfrac{\partial p}{\partial z}$ =-1.5 N/m^3
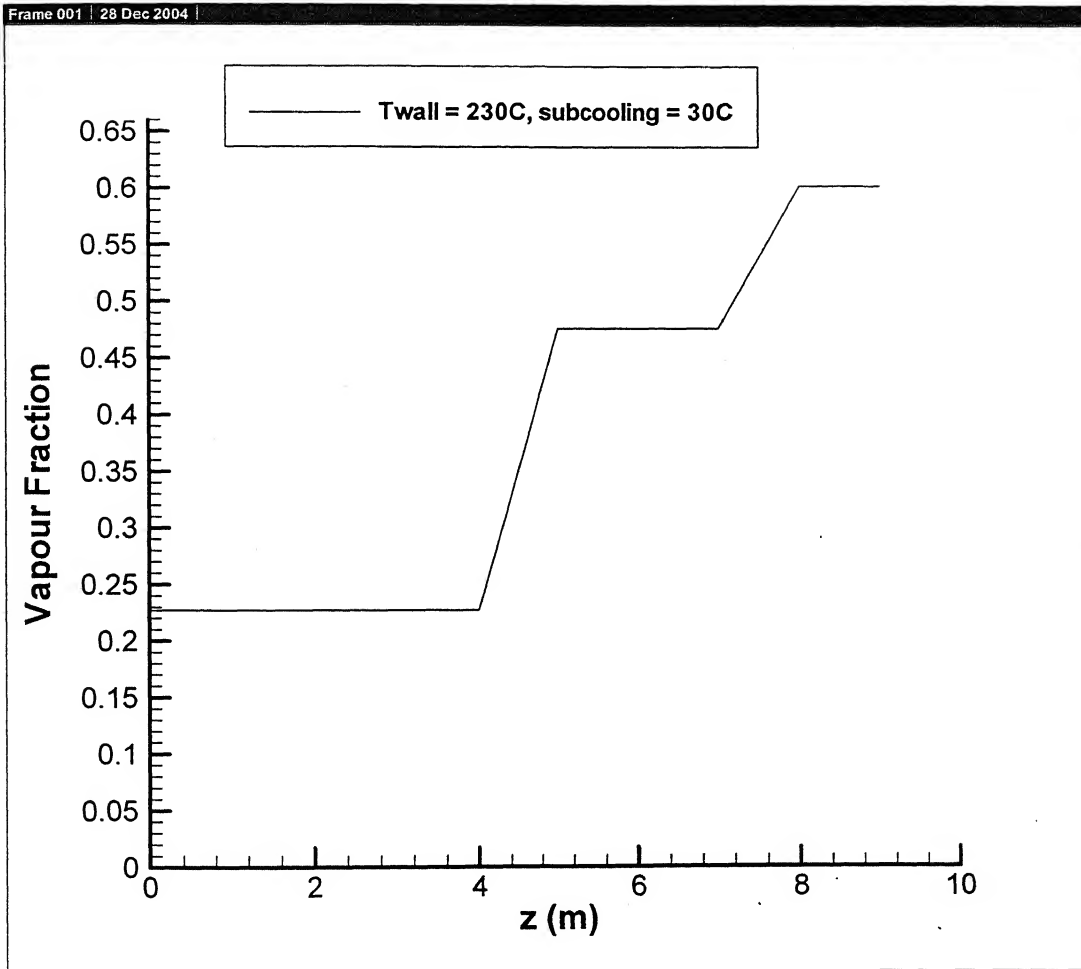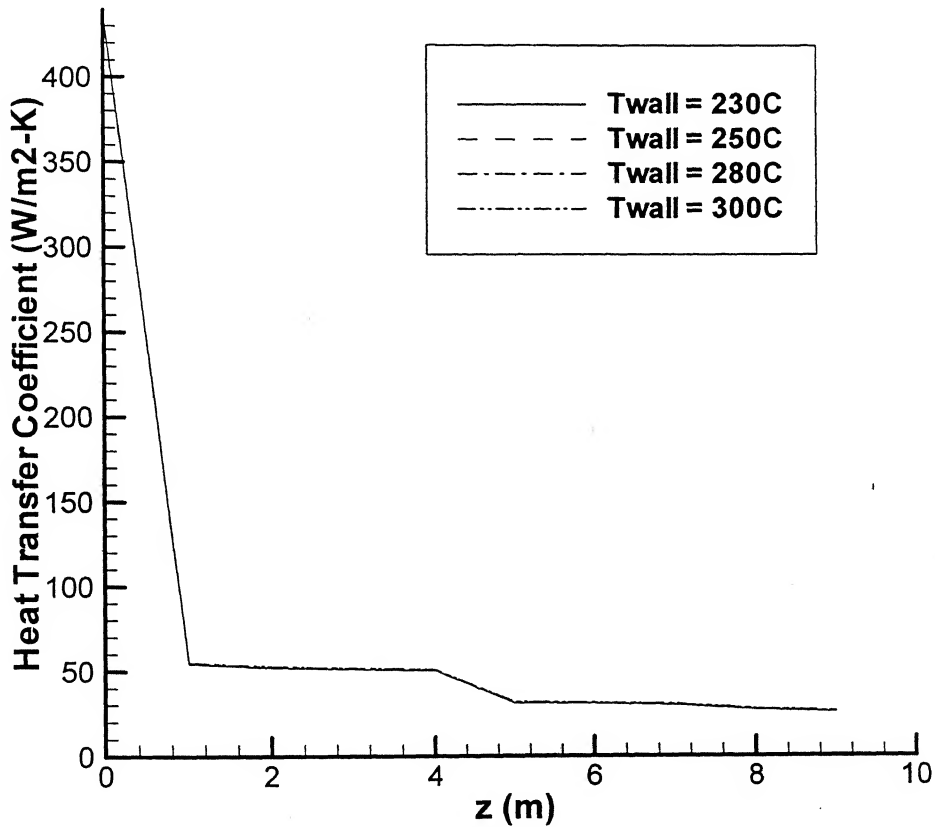
Fig.4.4 Vapour Fraction versus axial coordinate curve for Water $\dfrac{\partial p}{\partial z}$ =-1.5 N/m³

Fig. 4.5 Comparison of h $_{mean}$ vs. z curves for different wall temperatures and

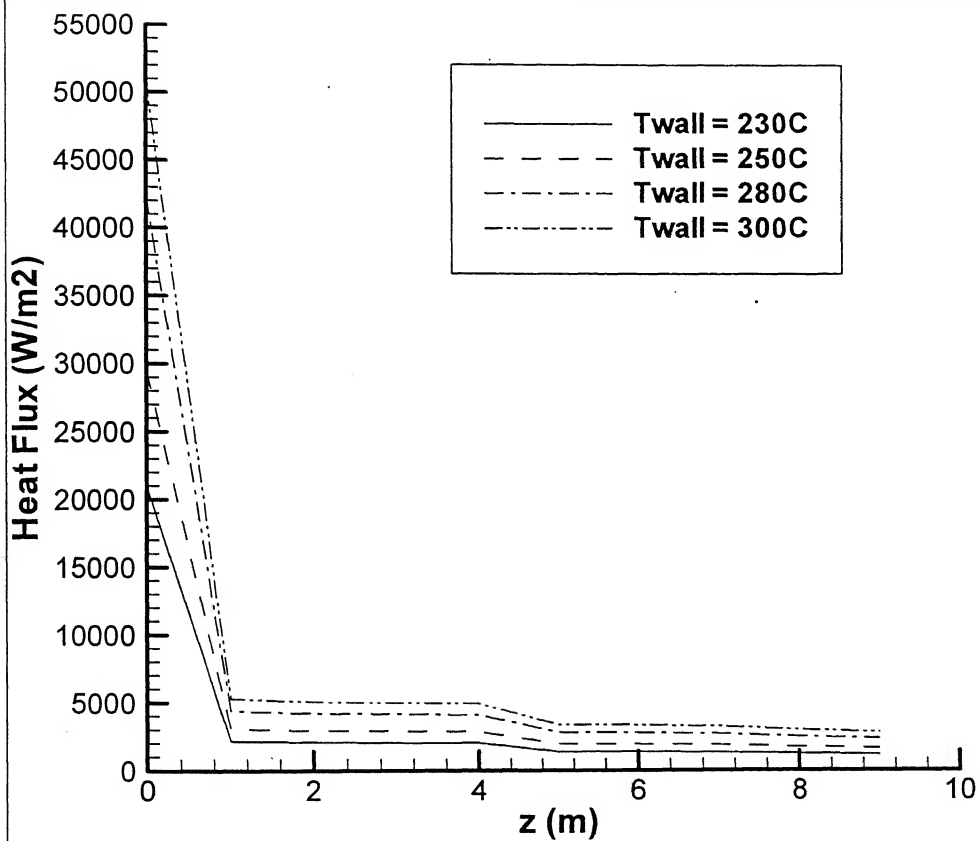at $\Delta T_{sub} = 30^0$C , $\frac{\partial p}{\partial z}$ =-1.5 N/m^3 for Water

Fig. 4.6 Comparison of q$''$ vs. z curves for different wall temperatures and at

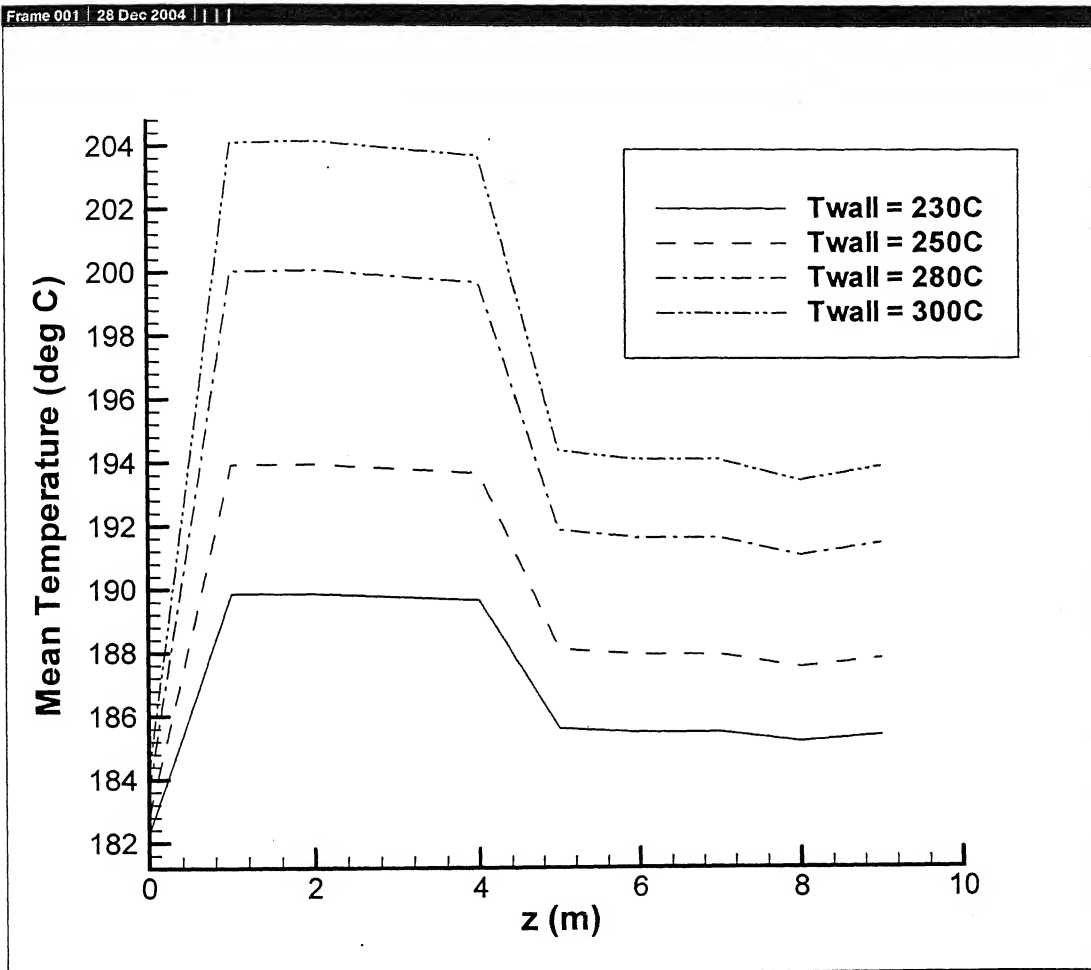$$\Delta T_{sub} = 30^0\text{C}, \frac{\partial p}{\partial z} = -1.5 \text{ N/m}^3 \text{ for Water}$$

Fig. 4.7 Comparison of T_{mean} vs. z for different wall temperature at $\Delta T_{sub} = 30^0C$, $\dfrac{\partial p}{\partial z} = -1.5$ N/m^3 for Water
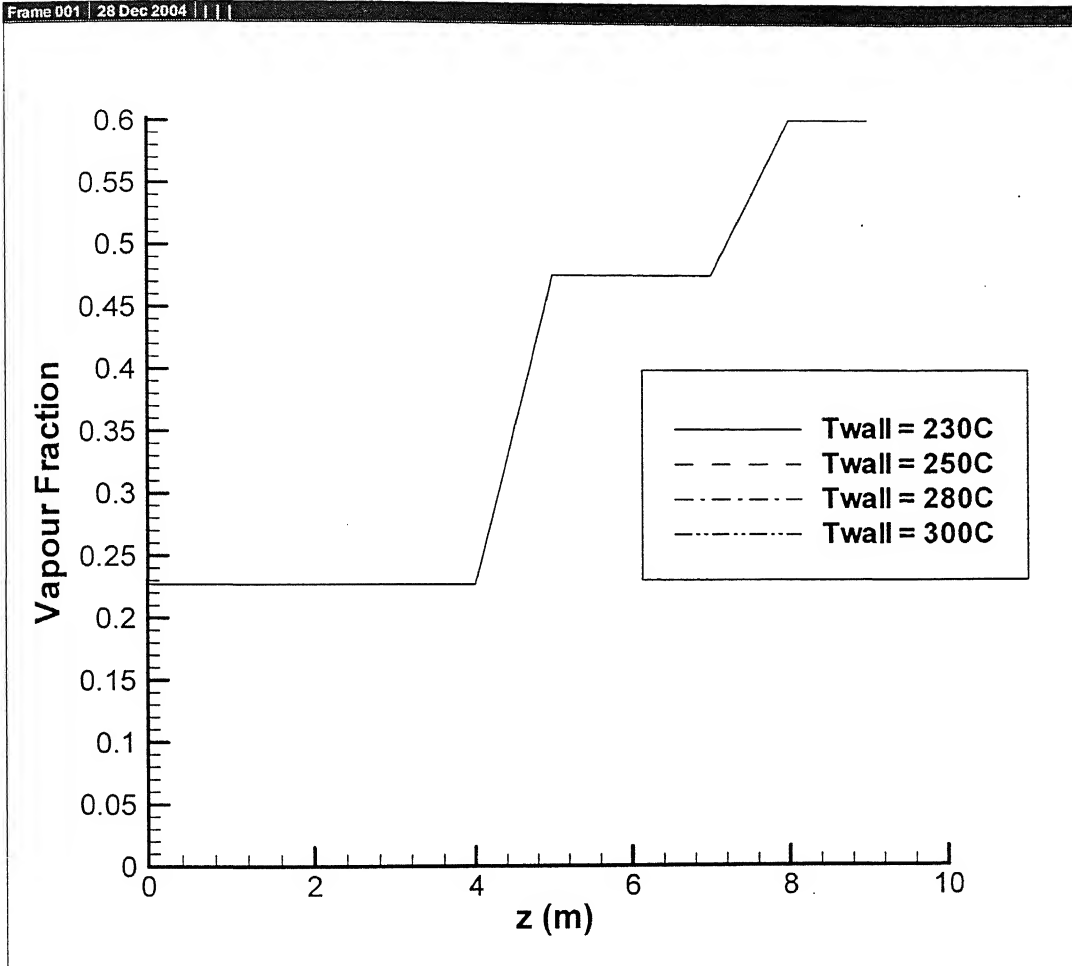
Fig. 4.8 Comparison of f vs. z curves for different wall temperatures

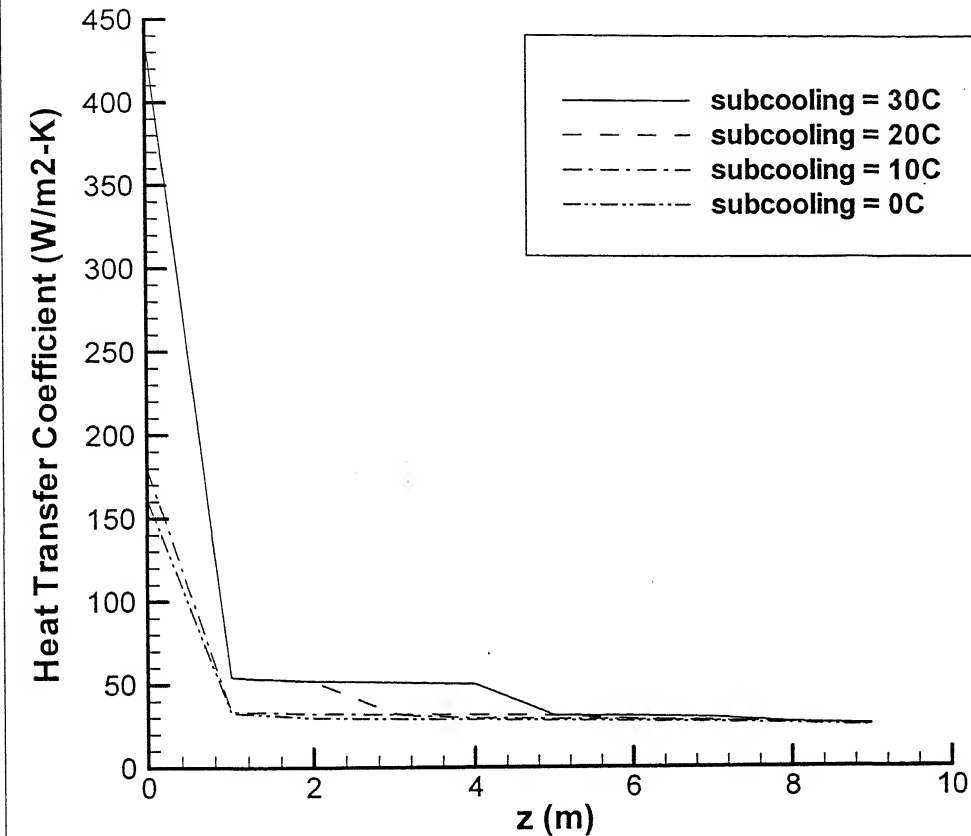and at $\Delta T_{sub} = 30^0\text{C}$, $\dfrac{\partial p}{\partial z} = -1.5 \text{ N/m}^3$ for Water

Fig.4.9 Comparison of h $_{mean}$ vs. z curves for different ΔT_{sub} at constant wall temperature (Twall = 230 ^{0}C), $\dfrac{\partial p}{\partial z}$ = -1.5 N/m^3 for Water
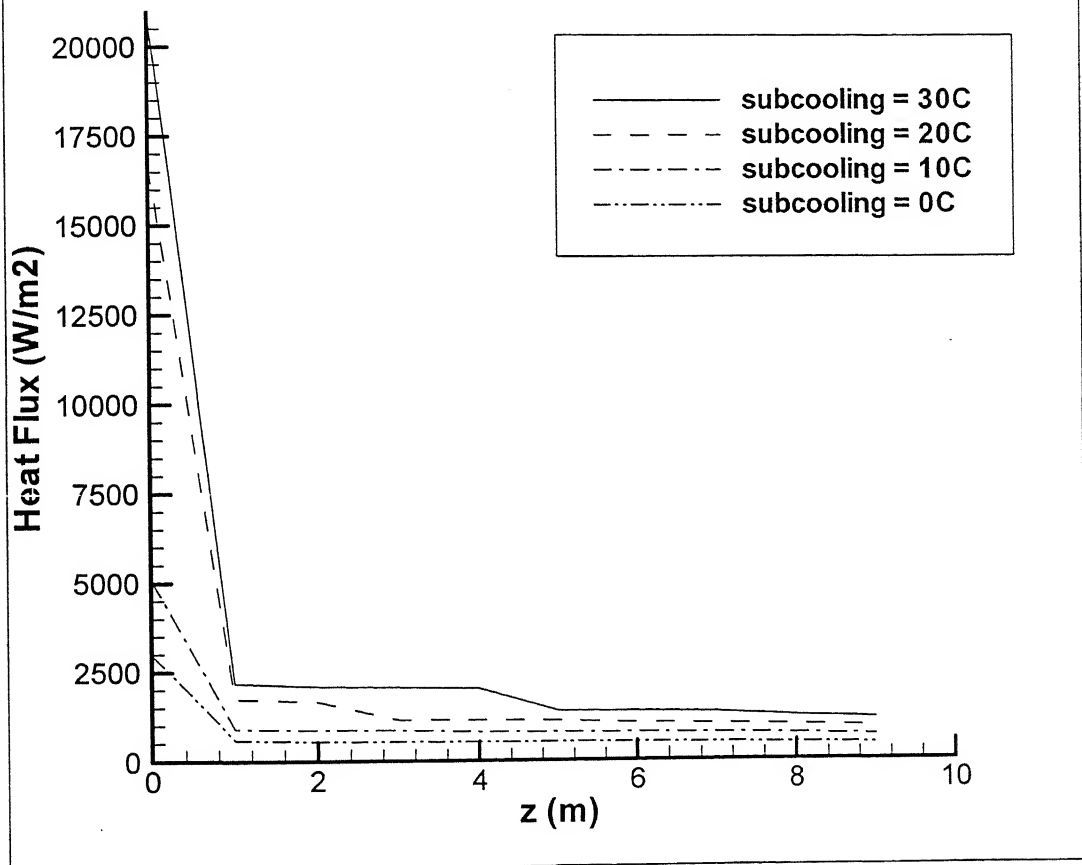
Fig.4.10 Comparison of q$^{//}$ vs. z curves for different ΔT_{sub} at constant wall

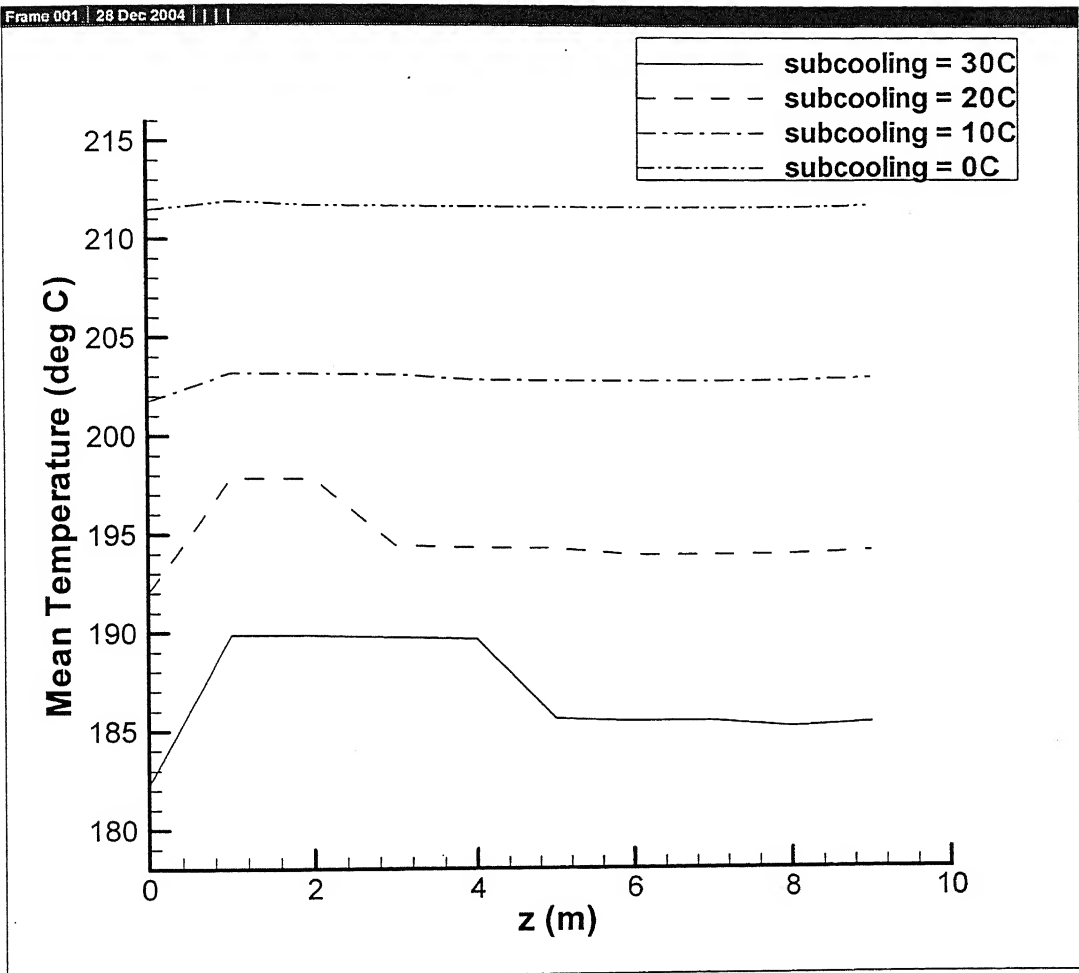temperature (Twall = 230^{0}C), $\dfrac{\partial p}{\partial z}$ =-1.5 N/m^{3} for Water

Fig.4.11 Comparison of T_{mean} vs. z for different ΔT_{sub} at constant wall temperature (Twall = 230^{0}C), $\dfrac{\partial p}{\partial z}$ = -1.5 N/m^3 for Water
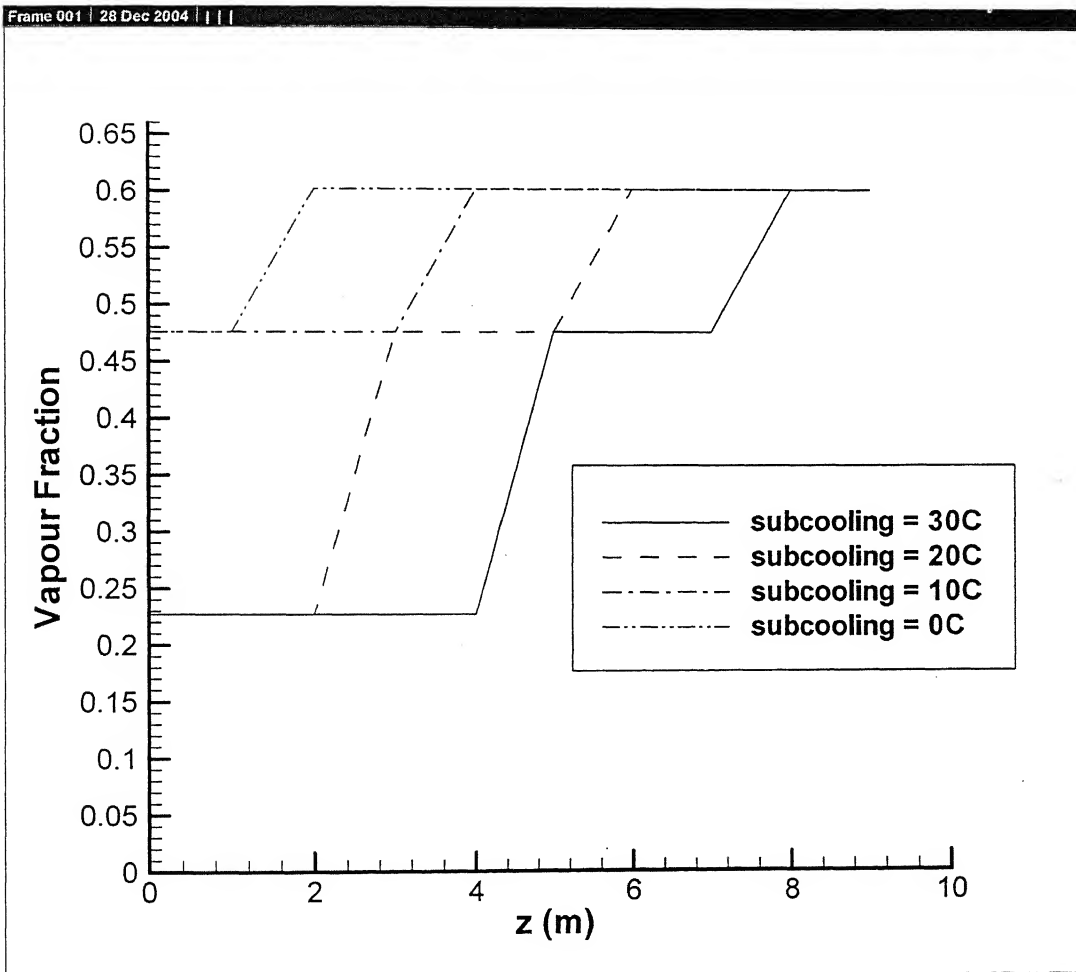
Fig.4.12 Comparison of f vs. z curve for different ΔT_{sub} at constant wall temperature

(Twall = $230\,^{0}$C), $\dfrac{\partial p}{\partial z}$ = -1.5 N/m³ for Water

Fig.4.13 Comparison of h $_{mean}$ vs. z curves for different mass flow rates

And at constant wall temperature ($T_{wall} = 230\,^0C$), $\Delta T_{sub} = 30^0C$,

for Water

Fig.4.14 Comparison of q'' vs. z curves for different mass flow rates
and at constant wall temperature ($T_{wall} = 230\,^0\text{C}$), $\Delta T_{sub} = 30^0\text{C}$,
for Water
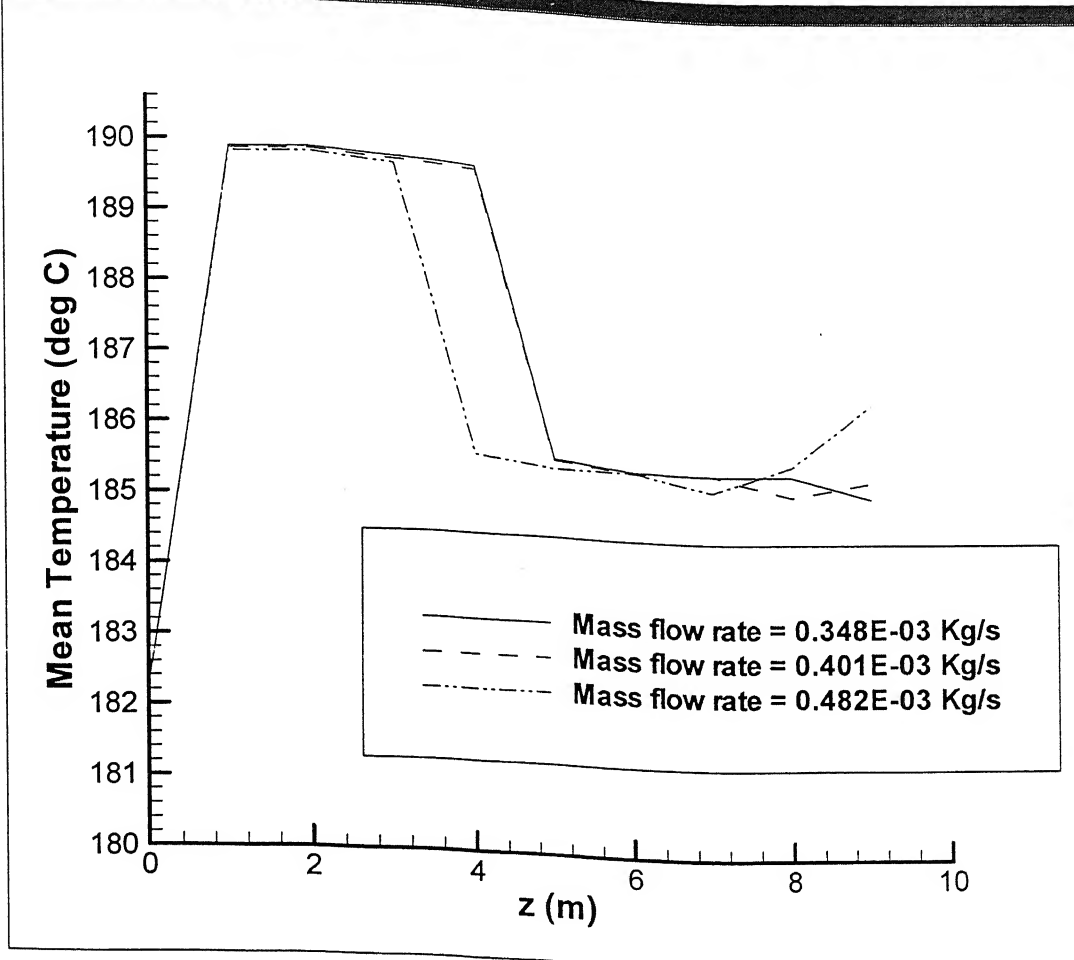
Fig.4.15 Comparison of T_{mean} vs. z for different mass flow rates and at constant wall temperature ($T_{wall} = 230\,^0C$), $\Delta T_{sub} = 30^0C$, for Water
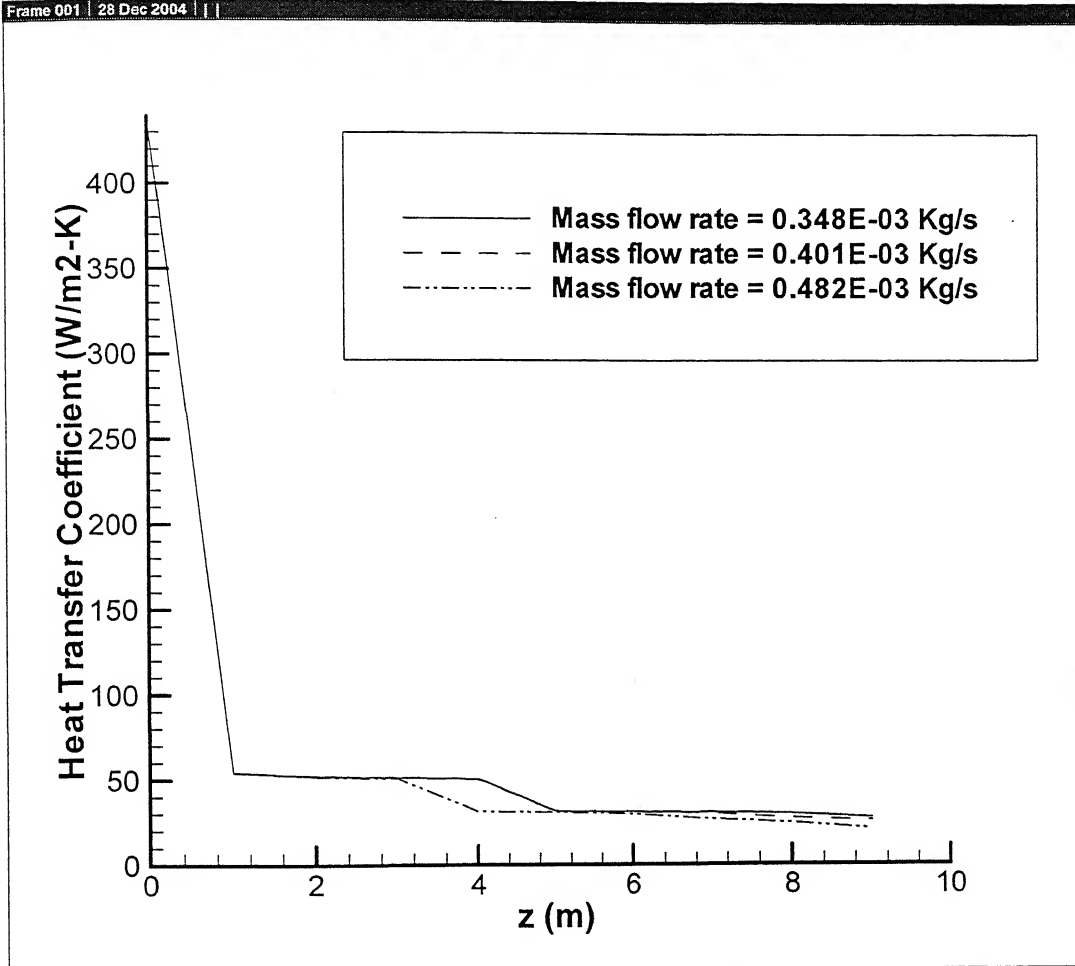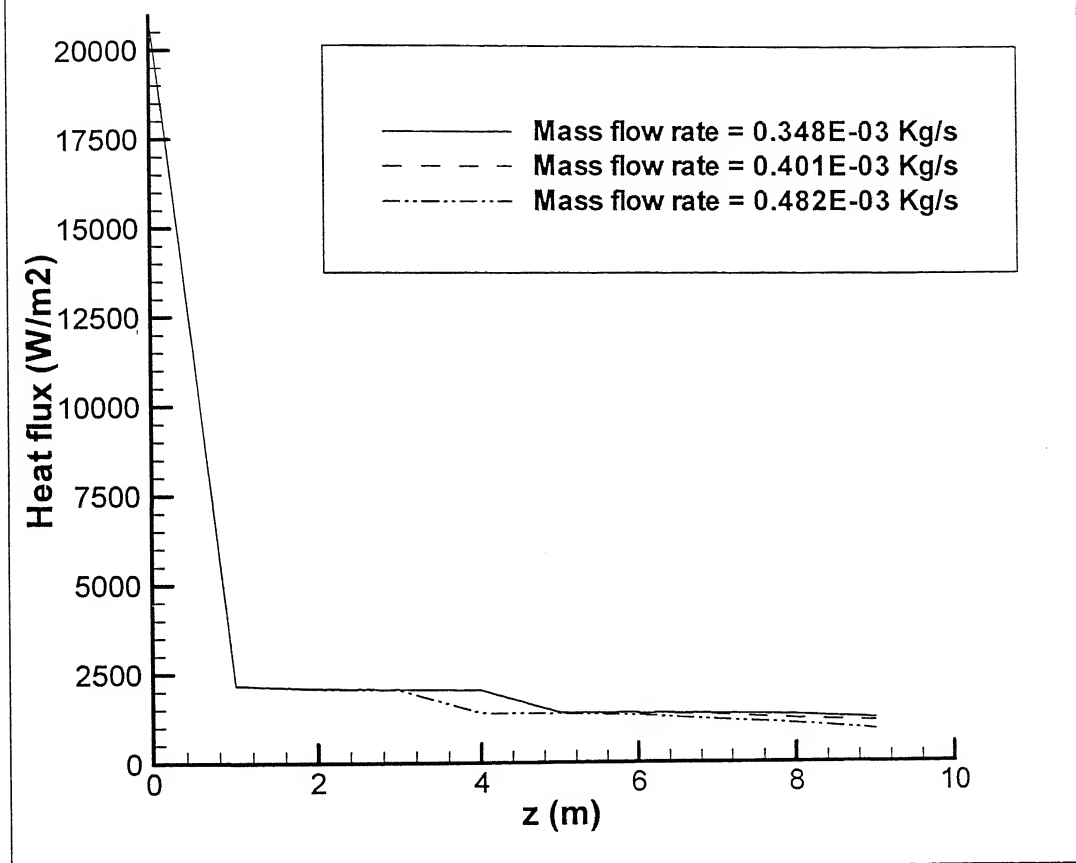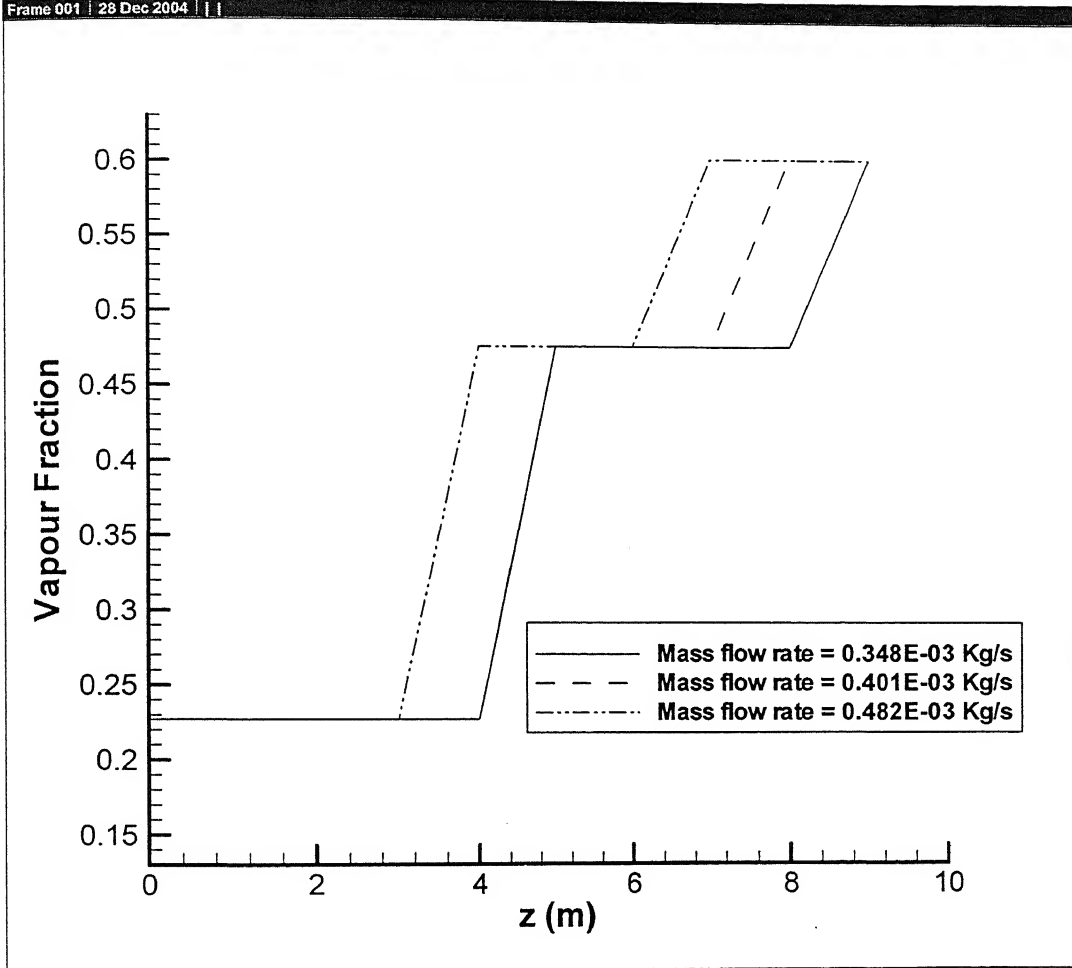
Fig.4.16 Comparison of f vs z curve for different mass flow rates
and at constant wall temperature ($T_{wall} = 230\,^0C$), $\Delta T_{sub} = 30^0C$,
for Water
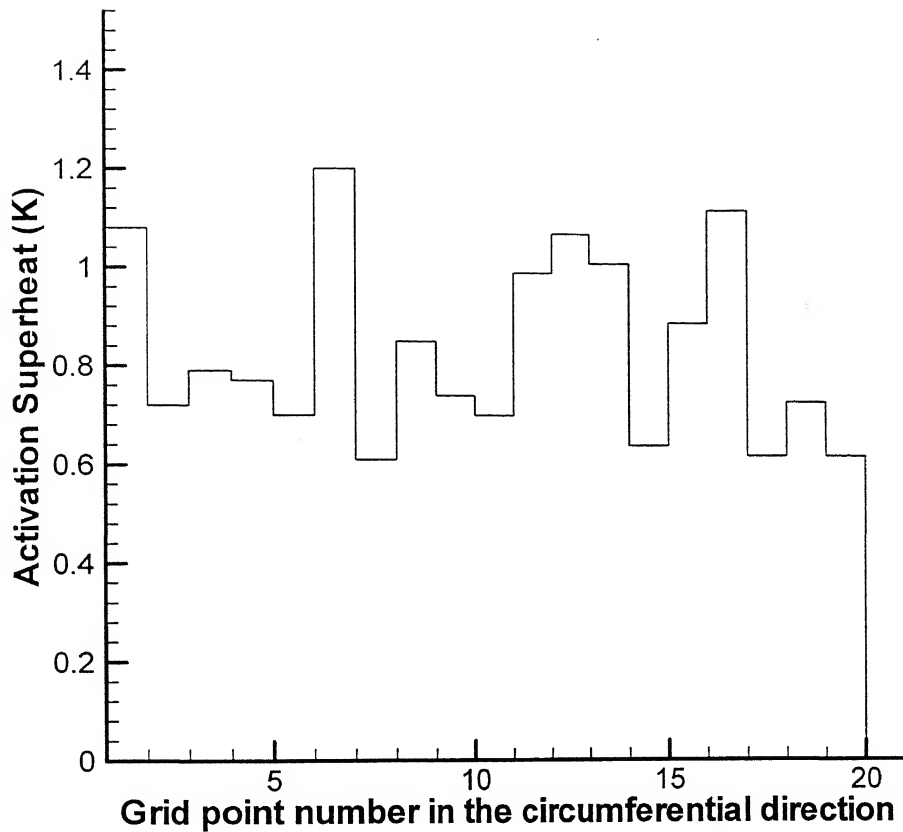
Fig.4.17 Circumferential Nucleation Superheat Distribution for Propane at the tube
entrance
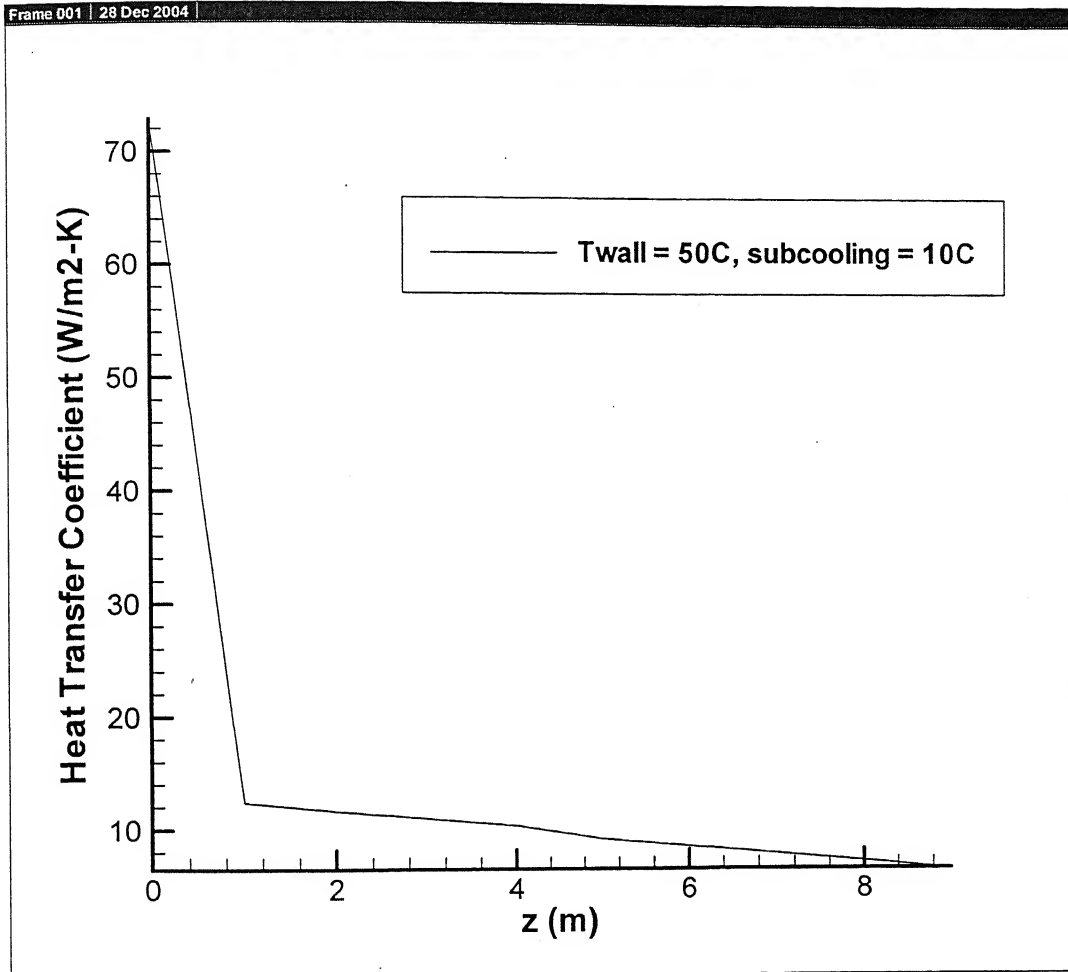
Fig 4.18 Heat Transfer Coefficient versus axial coordinate curve for Propane
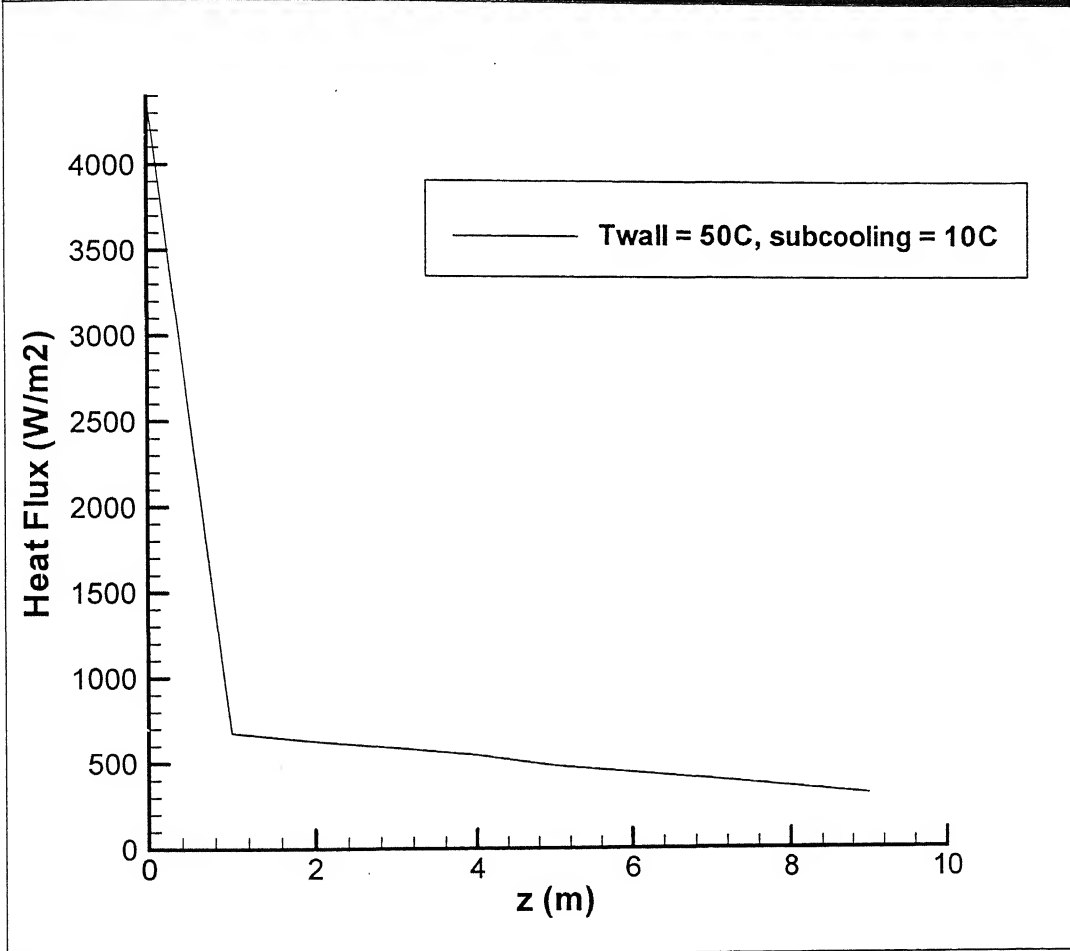
$$\frac{\partial p}{\partial z} = -.3 \text{ N/m}^3$$

Fig 4.19 Heat Flux versus axial coordinate curve for propane $\dfrac{\partial p}{\partial z} = -.3$ N/m^3
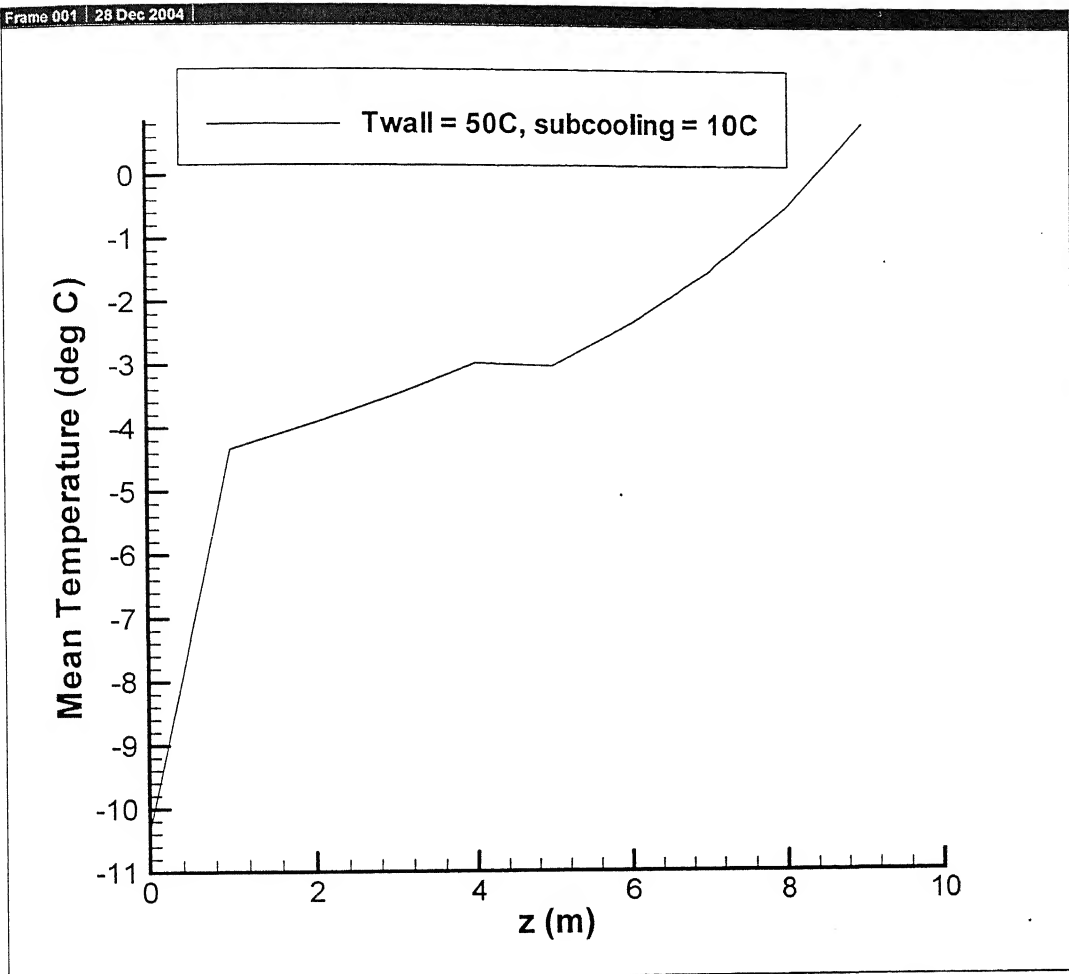
Fig. 4.20 Mean temperature of fluid (Tmean) versus axial coordinate curve for
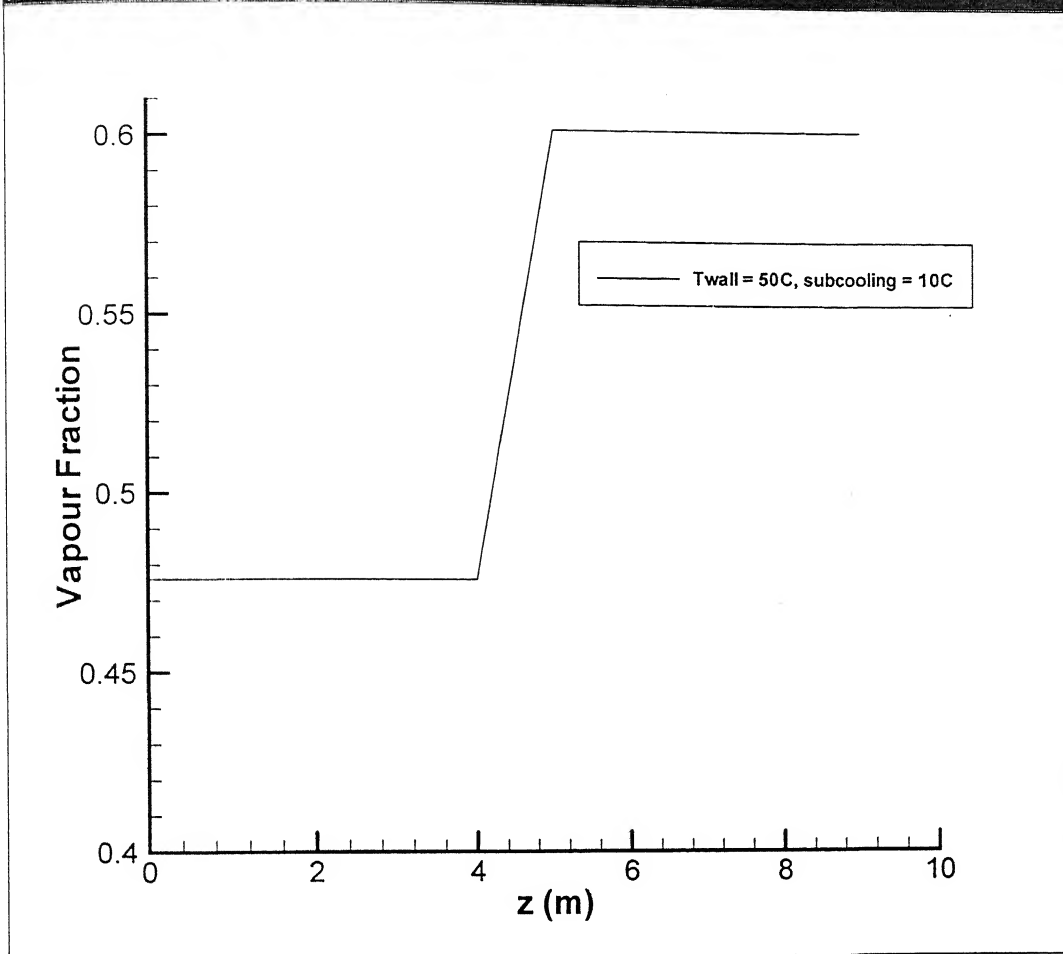
Propane $\dfrac{\partial p}{\partial z} = -.3 \ \text{N/m}^3$

Fig.4.21 Vapour Fraction versus axial coordinate curve for Propane $\dfrac{\partial p}{\partial z} = -.3 \text{ N/m}^3$
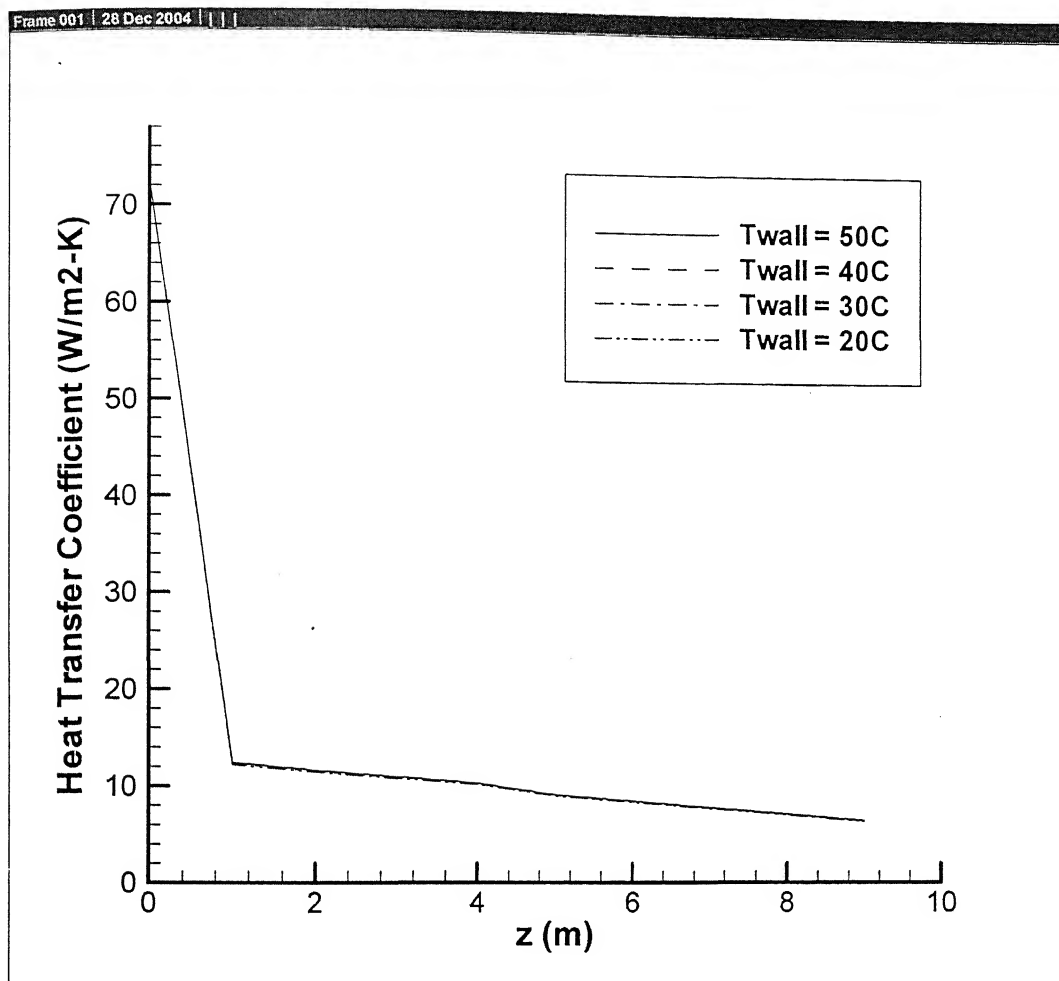
Fig. 4.22 Comparison of h_{mean} vs. z curves for different wall temperatures and

at $\Delta T_{sub} = 10^{0}\text{C}$, $\frac{\partial p}{\partial z} = -.3 \text{ N/m}^3$ for Propane
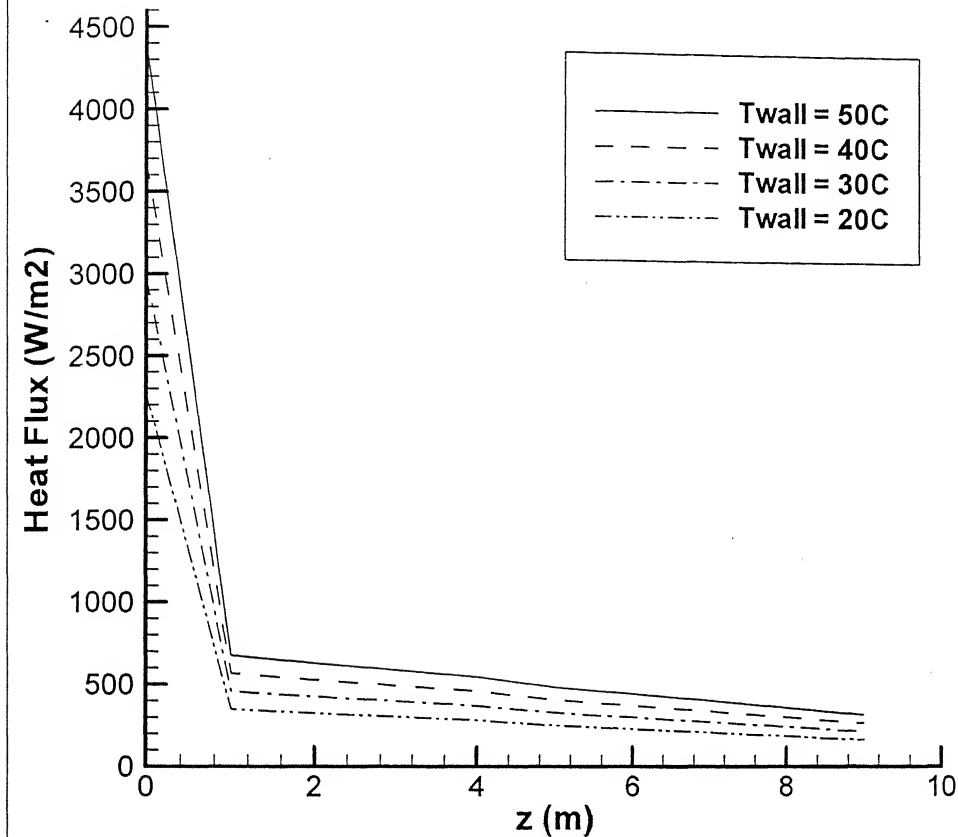
Fig. 4.23 Comparison of q'' vs. z curves for different wall temperatures and at $\Delta T_{sub} = 10^0$C, $\dfrac{\partial p}{\partial z} = -.3$ N/m^3 for Propane

49
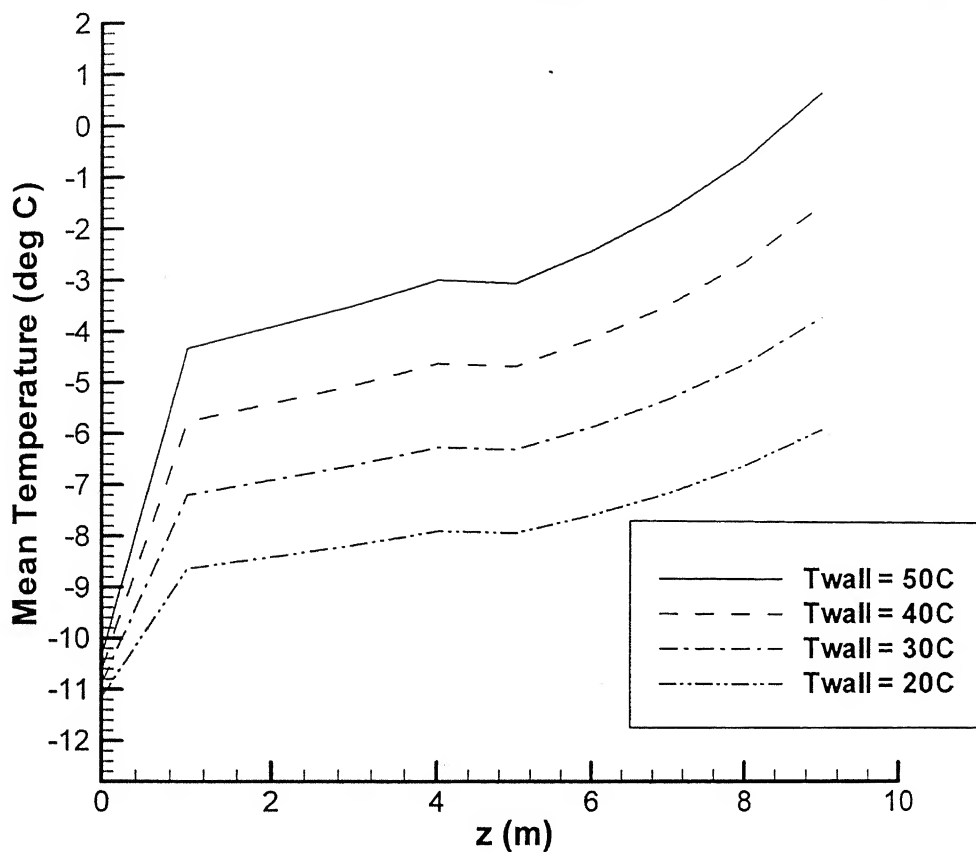
Fig. 4.24 Comparison of T$_{mean}$ vs. z for different wall temperature at $\Delta T_{sub} = 10^0C$, $\frac{\partial p}{\partial z}$ =-.3 N/m^3 for Propane
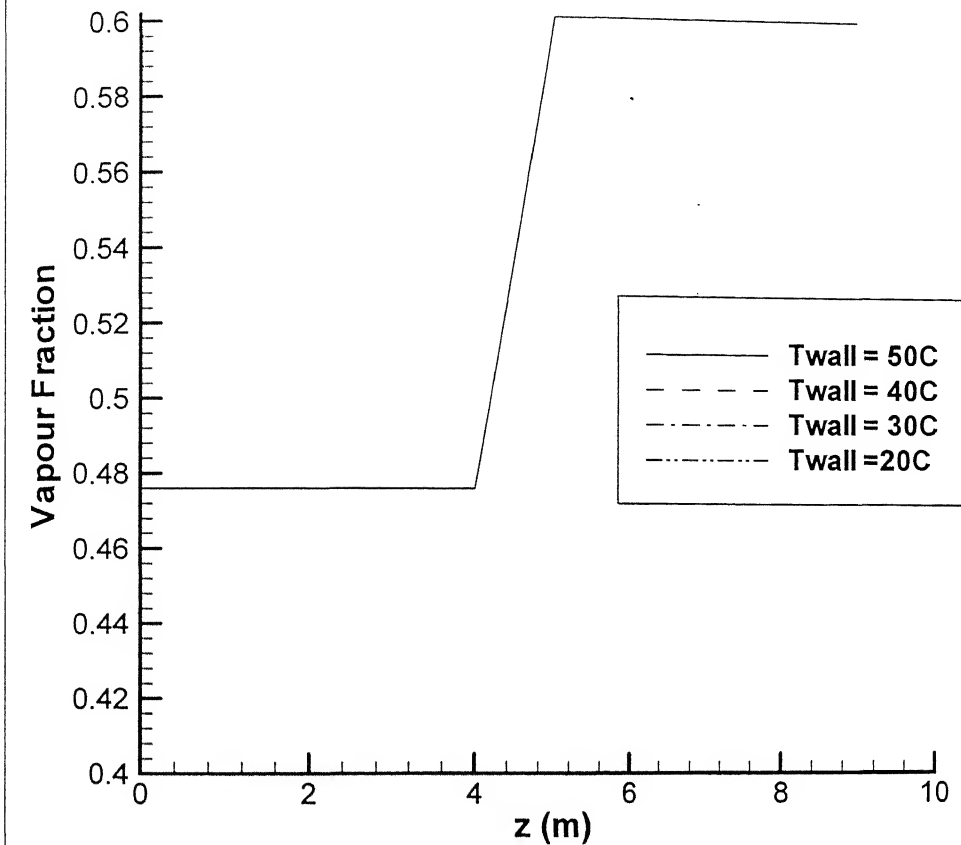
Fig. 4.25 Comparison of f vs. z curves for different wall temperatures

and at $\Delta T_{sub} = 10^0 C$, $\frac{\partial p}{\partial z} = -.3$ N/m^3 for Propane
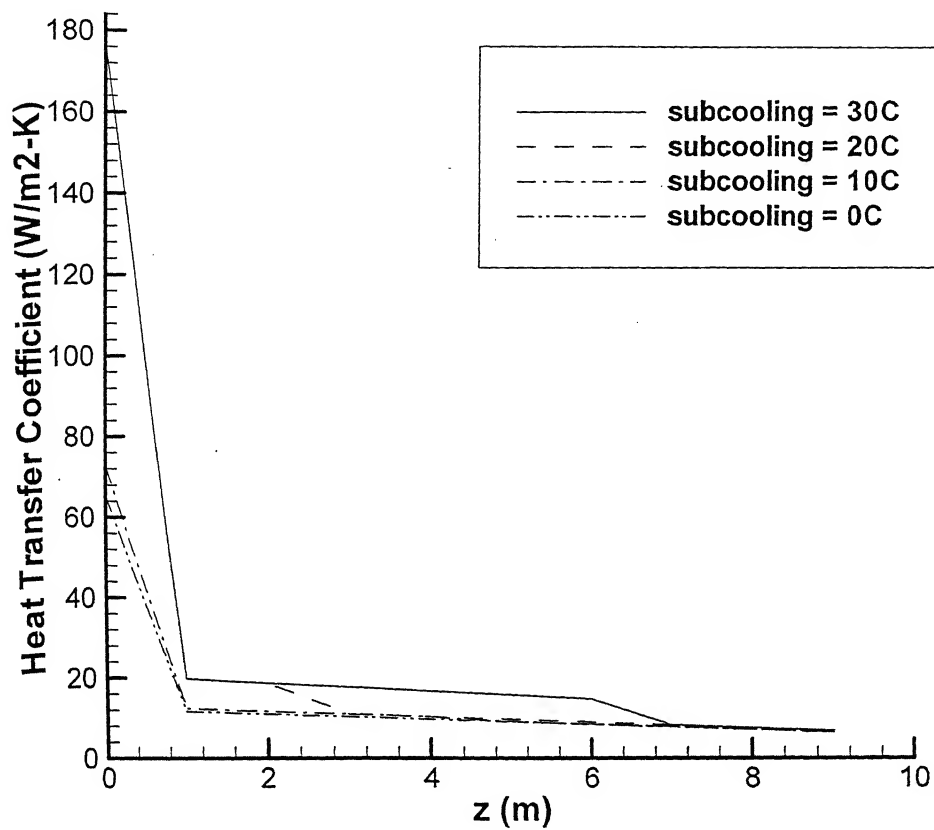
Fig.4.26 Comparison of h_{mean} vs. z curves for different ΔT_{sub} at constant wall temperature (Twall $= 40\,^0$C), $\dfrac{\partial p}{\partial z} = -.3$ N/m^3 for Propane
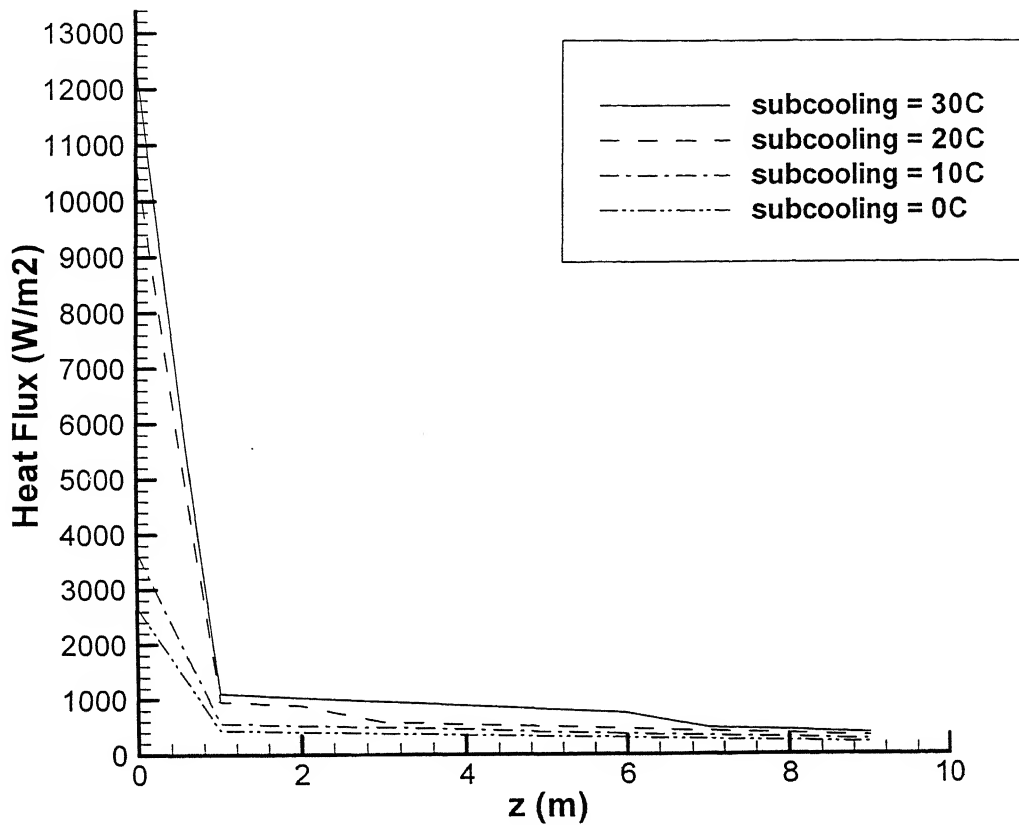
Fig.4.27 Comparison of q'' vs. z curves for different ΔT_{sub} at constant wall temperature (Twall = 40 ^{0}C), $\dfrac{\partial p}{\partial z}$ =-.3 N/m^3 for Propane
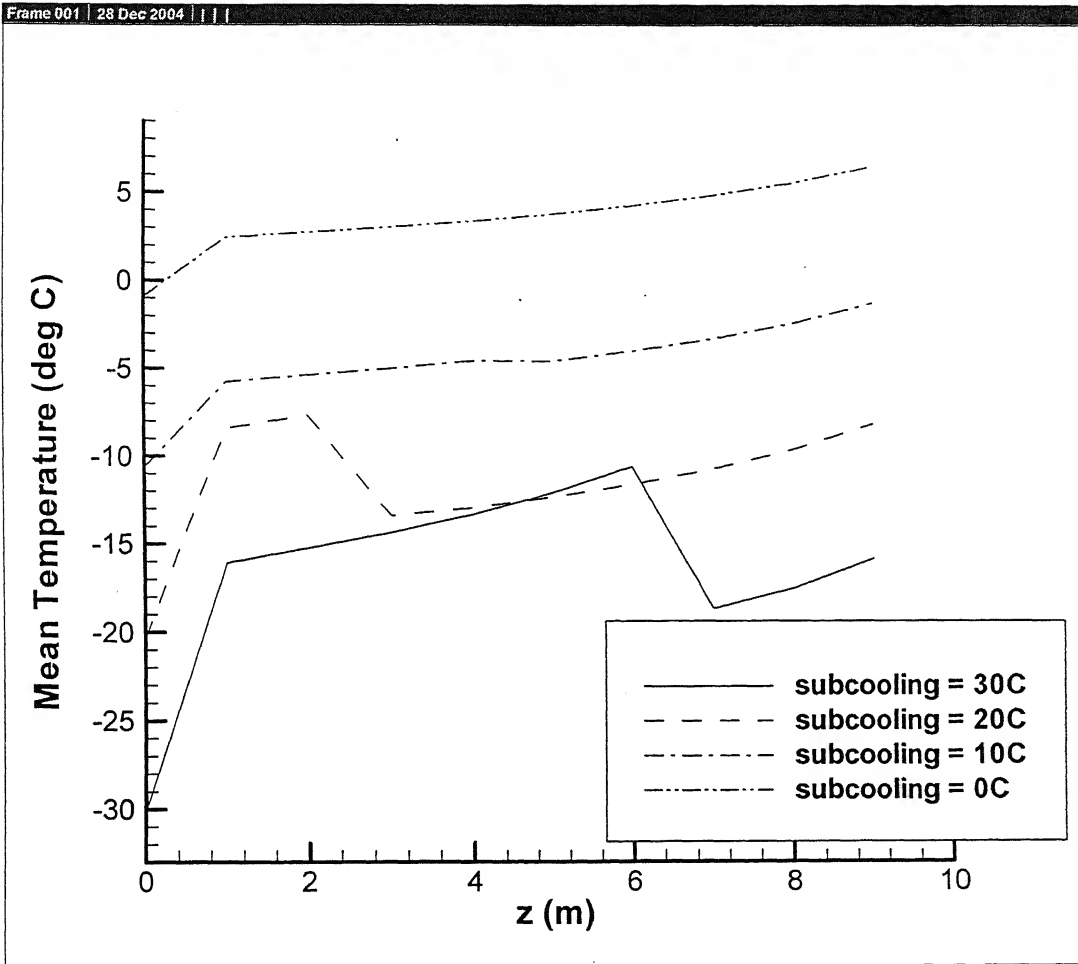
Fig.4.28 Comparison of T$_{mean}$ vs. z for different ΔT_{sub} at constant wall temperature (Twall = 40^{0}C), $\dfrac{\partial p}{\partial z}$ =-.3 N/m^3 for Propane
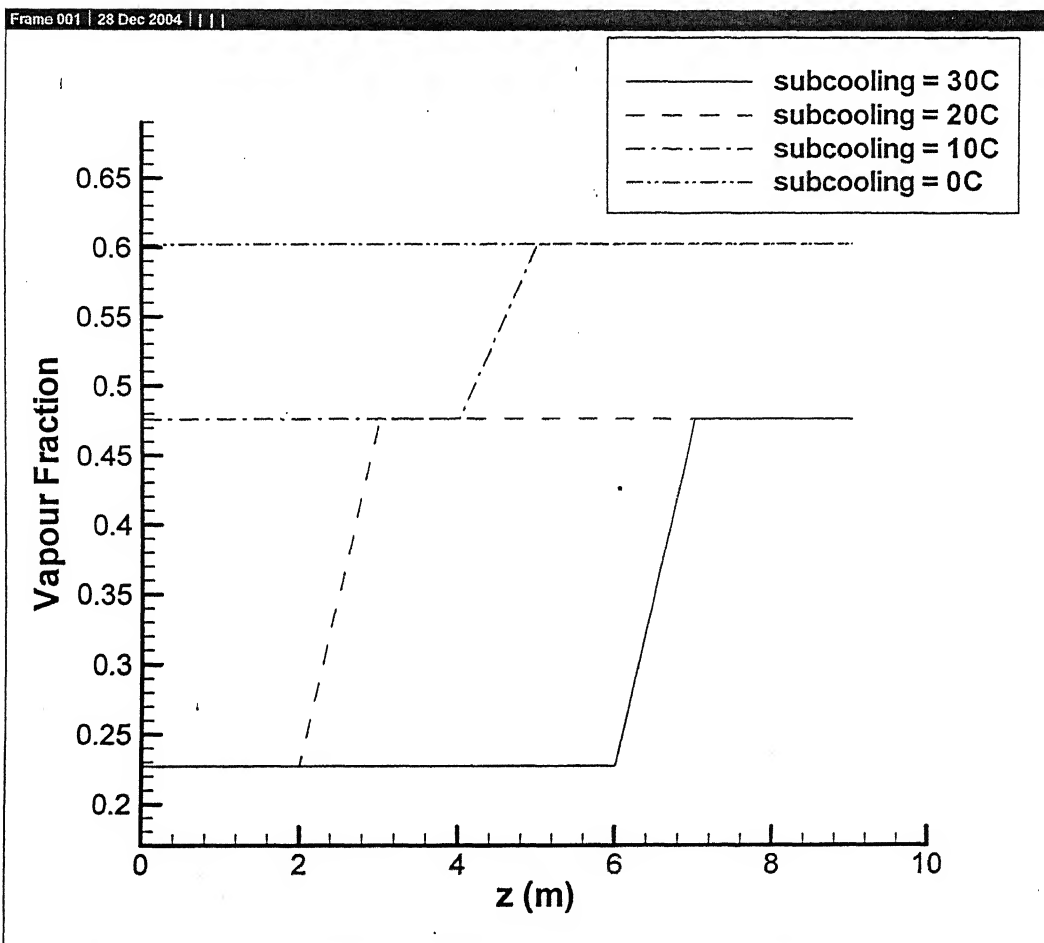
Fig.4.29 Comparison of f vs. z curve for different ΔT_{sub} at constant wall temperature

(Twall = $40\,^0$C), $\dfrac{\partial p}{\partial z}$ =-0.3 N/m^3 for Propane
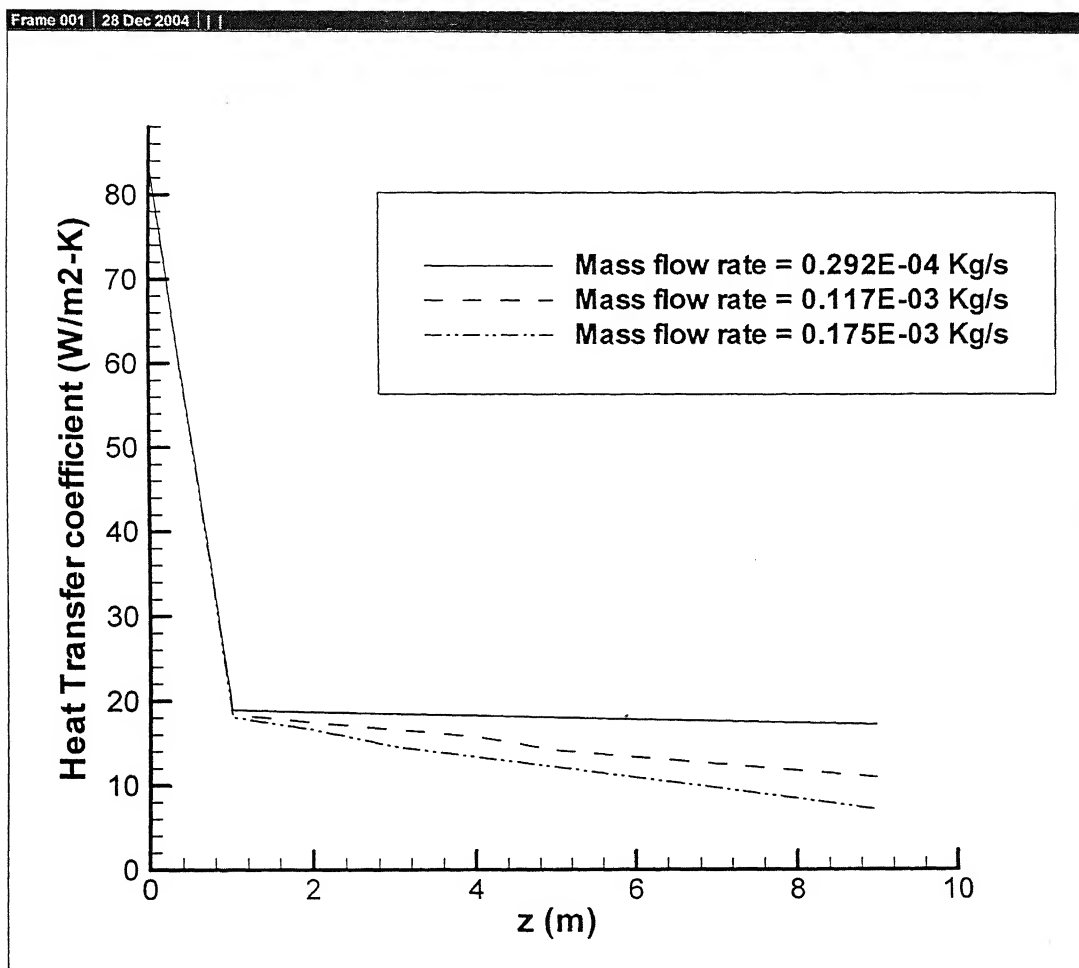
Fig.4.30 Comparison of h $_{mean}$ vs. z curves for different mass flow rates
and at constant wall temperature ($T_{wall} = 40\,^{0}C$), $\Delta T_{sub} = 10^{0}C$,
for Propane

Fig.4.31 Comparison of q'' vs. z curves for different mass flow rates
and at constant wall temperature ($T_{wall} = 40^0 C$), $\Delta T_{sub} = 10^0 C$,
for Propane

57

Fig.4.32 Comparison of T_{mean} vs. z for different mass flow rates
and at constant wall temperature ($T_{wall} = 40^0 C$), $\Delta T_{sub} = 10^0 C$,
for Propane

Fig.4.33 Comparison of f vs z curve for different mass flow rates
and at constant wall temperature ($T_{wall} = 40^{\circ} C$), $\Delta T_{sub} = 10^{0} C$,
for Propane

CHAPTER 5

CONCLUSIONS AND SCOPE FOR FUTURE WORK

The present work shows the modelling of laminar, non – stratified flow boiling of water and propane in a constant wall temperature horizontal tube by the coupled map lattice method (CML). It may be noted that CML s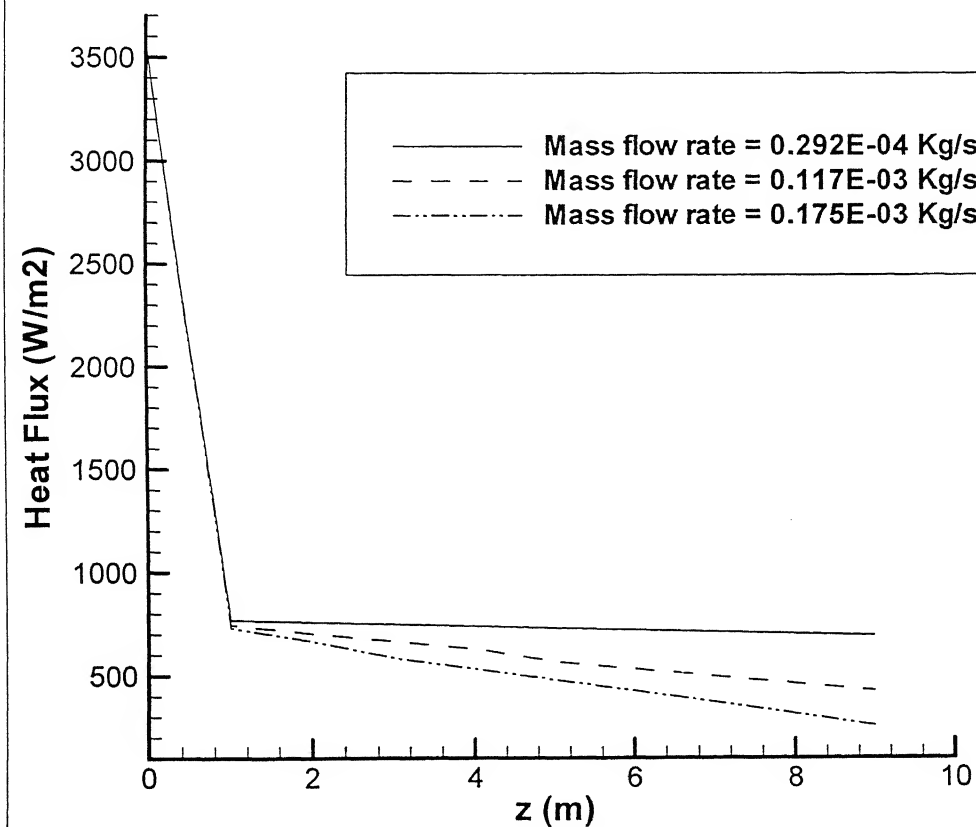imulation produces only qualitative results. However, the simulation by CML is very useful to get an insight into complex phenomena such as boiling which can not be handled by available CFD techniques. The results are presented for variation of heat transfer coefficient, heat flux, mean fluid temperature and vapour fraction along the axial coordinate of the tube. The main observations from the results are the following, (i) The wall temperature does not affect the heat transfer coefficient and vapour fraction; (ii) The decrease in entry subcooling lowers the heat transfer coefficient near the tube entrance but does not influence the heat transfer coefficient in the latter part of the tube. Furthermore, vapor fraction is high near the tube entrance for low ΔT_{sub}'s whereas the maximum vapour fraction is same for all ΔT_{sub}'s. (iii) The heat transfer coefficient is virtually independent of mean flow rate in the initial section of the tube where the nucleate boiling effect is dominant. On the other hand, in the latter part of the tube where the convection vapourization is significant, because heat transfer coefficient falls with increase in mass flow rate. All these trends are similar for both water and propane.

An exception for propane is noted where it is seen that fluid mean temperature is higher for $\Delta T_{sub} = 20^{o}C$ than for $\Delta T_{sub} = 30^{o}C$ in the section of the tube from z = 4.8m to 6m. Another difference with respect to water is that the convective vapourization zone much larger as compared to the zone where the nucleate boiling is dominant. In addition to the above, the drop in heat transfer coefficient at some location down the tube is not as marked as that for water.

The present analysis can be extended to include turbulent flow boiling (turbulent liquid, turbulent vapour) in a horizontal tube as turbulence is commonly encountered in industrial flow boiling.

APPENDIX A

Finite difference based Method of Solution
of Momentum and Energy Equations

A.1 Handling of the condition at the centre

Fig. A.1 shows the grid in the r - θ plane of the computational domain. Fig. A.2 shows grid lines in the z – direction.

Recall the z – momentum and energy equations.

z – Momentum:

$$\rho \frac{\partial v_z}{\partial t} + \rho v_z \frac{\partial v_z}{\partial z} = -\frac{\partial p}{\partial z} + \mu \frac{1}{r} \frac{\partial}{\partial r} (r \frac{\partial v_z}{\partial r}) + \mu \frac{1}{r^2} \frac{\partial^2 v_z}{\partial \theta^2} \qquad (A.1)$$

Energy:

$$\rho c_p \frac{\partial T}{\partial t} + \rho c_p v_z \frac{\partial T}{\partial z} = k_f \left[\frac{1}{r} \frac{\partial}{\partial r} (r \frac{\partial T}{\partial r}) \right] + \frac{k_f}{r^2} \frac{\partial^2 T}{\partial \theta^2} \qquad (A.2)$$

It can be clearly seen from Eqs. (A.1) and (A.2) that 2nd and 3rd terms of Eq. (A.1) and 1st and 2nd terms of Eq. (A.2) become infinity at r = 0, leading to an undesirable situation. But, since at r = 0, neither $\frac{\partial v_z}{\partial r}$ nor $\frac{\partial T}{\partial r}$ is necessarily zero, l'Hospital's rule can not be applied. Furthermore, at r = 0, $\frac{\partial v_z}{\partial \theta}$ and $\frac{\partial T}{\partial \theta}$ do not exist. Therefore, a special treatment at r = 0 is obviously needed.

The aforesaid problem can be circumvented by taking a very small square region around the centre of the cylinder (see Fig. A.1) so that the governing differential equation in cartesian coordinates is valid in that region (Ghoshdastidar, 2004). The middle points of the top, bottom, right and left sides of the square will now coincide with the points on the horizontal and vertical lines passing through the centre of the circle (Fig. A.1).

Therefore, at r = 0, i.e. at (1, 1, k), the z – momentum and energy equations take the following forms.

z – Momentum:

$$\rho \frac{\partial v_z}{\partial t} + \rho v_z \frac{\partial v_z}{\partial z} = -\frac{\partial p}{\partial z} + \mu \left[\frac{\partial^2 v_z}{\partial x^2} + \frac{\partial^2 v_z}{\partial y^2} \right] \tag{A.3}$$

Energy:

$$\rho c_p \frac{\partial T}{\partial t} + \rho c_p v_z \frac{\partial T}{\partial z} = k_f \left[\frac{\partial^2 T}{\partial x^2} + \frac{\partial^2 T}{\partial y^2} \right] \tag{A.4}$$

Note $\Delta x = \Delta y = \Delta r$ in the square region. In the rest of the domain, r - θ system is used. The method is quite accurate, as in a small region around the centre, a circle almost coincides with a square. Hence, the solution in the cartesian geometry is a good approximation.

A.2 Discretization

Equations (A.1) – (A.4) are discretized using Explicit finite – difference scheme (Ghoshdastidar, 2004).

Discretizatized form of equation (A.1)

$$(\rho)^p_{(i,j,k+1)} \left[\frac{v^{p+1}_{z(i,j,k+1)} - v^p_{z(i,j,k+1)}}{\Delta t} \right] + (\rho)^p_{(i,j,k+1)} v^p_{z(i,j,k+1)} \left[\frac{v^p_{z(i,j,k+1)} - v^p_{z(i,j,k)}}{\Delta z} \right]$$

$$= -\left(\frac{\partial p}{\partial z} \right)^p_{(i,j,k+1)}$$

$$+ (\mu)^p_{(i,j,k+1)} \left[\frac{v^p_{z(i+1,j,k)} - 2v^p_{z(i,j,k)} + v^p_{z(i-1,j,k)}}{(\Delta r)^2} + \frac{1}{(r)_{(i,j,k+1)}} \frac{v^p_{z(i+1,j,k+1)} - v^p_{z(i-1,j,k+1)}}{2\Delta r} \right]$$

$$+ \frac{(\mu)^p_{(i,j,k+1)}}{\{(r)_{(i,j,k+1)}\}^2} \left[\frac{v^p_{z(i,j+1,k+1)} - 2v^p_{z(i,j,k+1)} + v^p_{z(i,j-1,k+1)}}{(\Delta \theta)^2} \right] \tag{A.5}$$

Valid for

$i = 2\ldots\ldots\ldots\ldots\ldots\ldots m$

$j = 1\ldots\ldots\ldots\ldots\ldots\ldots n$

$k = 1\ldots\ldots\ldots\ldots\ldots\ldots l\text{-}1$

Discretized form of equation (A.3)

$$(\rho)^p_{(1,j,k+1)} \left[\frac{v^{p+1}_{z(1,j,k+1)} - v^p_{z(1,j,k+1)}}{\Delta t} \right] + (\rho)^p_{(1,j,k+1)} v^p_{z(1,j,k+1)} \left[\frac{v^p_{z(1,j,k+1)} - v^p_{z(1,j,k)}}{\Delta z} \right]$$

$$= -\left(\frac{\partial p}{\partial z}\right)^p_{(1,j,k+1)} + \left(\mu\right)^p_{(1,j,k+1)}\left[\frac{v^p_{z(2,1,k+1)} - 2v^p_{z(1,1,k+1)} + v^p_{z(2,j3,k+1)}}{\left(\Delta x\right)^2}\right.$$

$$\left.+\frac{v^p_{z(2,j2,k+1)} - 2v^p_{z(1,1,k+1)} + v^p_{z(2,j4,k+1)}}{\left(\Delta y\right)^2}\right] \tag{A.6}$$

Note that $\Delta x = \Delta y = \Delta r$.

Discretized form of equation (A.2)

$$\left(\rho\right)^p_{(i,j,k+1)}\left(c_p\right)^p_{(i,j,k+1)}\left[\frac{T^{p+1}_{(i,j,k+1)} - T^p_{(i,j,k+1)}}{\Delta t}\right] + \left(\rho\right)^p_{(i,j,k+1)}\left(c_p\right)^p_{(i,j,k+1)}\left(v_z\right)^p_{(i,j,k+1)}\left[\frac{T^p_{(i,j,k+1)} - T^p_{(i,j,k)}}{\Delta z}\right]$$

$$= \left(k\right)^p_{(i,j,k+1)}\left[\frac{T^p_{(i+1,j,k+1)} - 2T^p_{(i,j,k+1)} + T^p_{(i-1,j,k+1)}}{\left(\Delta r\right)^2} + \frac{1}{\left(r\right)_{(i,j,k+1)}}\frac{T^p_{(i+1,j,k+1)} - T^p_{(i-1,j,k+1)}}{2\Delta r}\right]$$

$$+ \frac{\left(k\right)^p_{(i,j,k+1)}}{\left\{\left(r\right)_{(i,j,k+1)}\right\}^2}\left[\frac{T^p_{(i,j+1,k+1)} - 2T^p_{(i,j,k+1)} + T^p_{(i,j-1,k+1)}}{\left(\Delta\theta\right)^2}\right] \tag{A.7}$$

Valid for

i = 2………………….m

j = 1………………….n

k = 1………………….l-1

Discretized form of equation (A.4)

$$\left(\rho\right)^p_{(1,j,k+1)}\left(c_p\right)^p_{(1,j,k+1)}\left[\frac{T^{p+1}_{(1,j,k+1)} - T^p_{(1,j,k+1)}}{\Delta t}\right] + \left(\rho\right)^p_{(1,j,k+1)}\left(c_p\right)^p_{(1,j,k+1)}\left(v_z\right)^p_{(1,j,k+1)}\left[\frac{T^p_{(1,j,k+1)} - T^p_{(1,j,k)}}{\Delta z}\right]$$

$$= \left(k\right)^p_{(1,j,k+1)}\left[\frac{T^p_{(2,1,k+1)} - 2T^p_{(1,1,k+1)} + T^p_{(2,j3,k+1)}}{\left(\Delta x\right)^2} + \frac{T^p_{(2,j2,k+1)} - 2T^p_{(1,1,k+1)} + T^p_{(2,j4,k+1)}}{\left(\Delta y\right)^2}\right] \tag{A.8}$$

Note that $\Delta x = \Delta y = \Delta r$.

A.3 Stability

In order to ensure stability of the numerical solution Δt must be governed by the following equations.

From equation (A.5)

$$\Delta t \leq \frac{1}{\left[\dfrac{v^p_{z(i,j,k+1)}}{\Delta z} - \dfrac{2(\mu)^p_{(i,j,k+1)}}{(\rho)^p_{(i,j,k+1)}}\left(\dfrac{1}{(\Delta r)^2} + \dfrac{1}{(r_{(i,j,k+1)})^2(\Delta \theta)^2}\right)\right]}, \quad \text{valid for } i > 1 \qquad (A.9)$$

From equation (A.6)

$$\Delta t \leq \frac{1}{\left[\dfrac{v^p_{z(1,1,k+1)}}{\Delta z} - \dfrac{2(\mu)^p_{(1,1,k+1)}}{(\rho)^p_{(1,1,k+1)}}\left(\dfrac{1}{(\Delta x)^2} + \dfrac{1}{(\Delta y)^2}\right)\right]} \qquad (A.10)$$

From equation (A.7)

$$\Delta t \leq \frac{1}{\left[\dfrac{v^p_{z(i,j,k+1)}}{\Delta z} - \dfrac{2(k_f)^p_{(i,j,k+1)}}{(\rho c_p)^p_{(i,j,k+1)}}\left(\dfrac{1}{(\Delta r)^2} + \dfrac{1}{(r_{(i,j,k+1)})^2(\Delta \theta)^2}\right)\right]}, \quad \text{valid for } i > 1 \qquad (A.11)$$

From equation (A.8)

$$\Delta t \leq \frac{1}{\left[\dfrac{v^p_{z(1,1,k+1)}}{\Delta z} - \dfrac{2(k_f)^p_{(1,1,k+1)}}{(\rho c_p)^p_{(1,1,k+1)}}\left(\dfrac{1}{(\Delta x)^2} + \dfrac{1}{(\Delta y)^2}\right)\right]} \qquad (A.12)$$
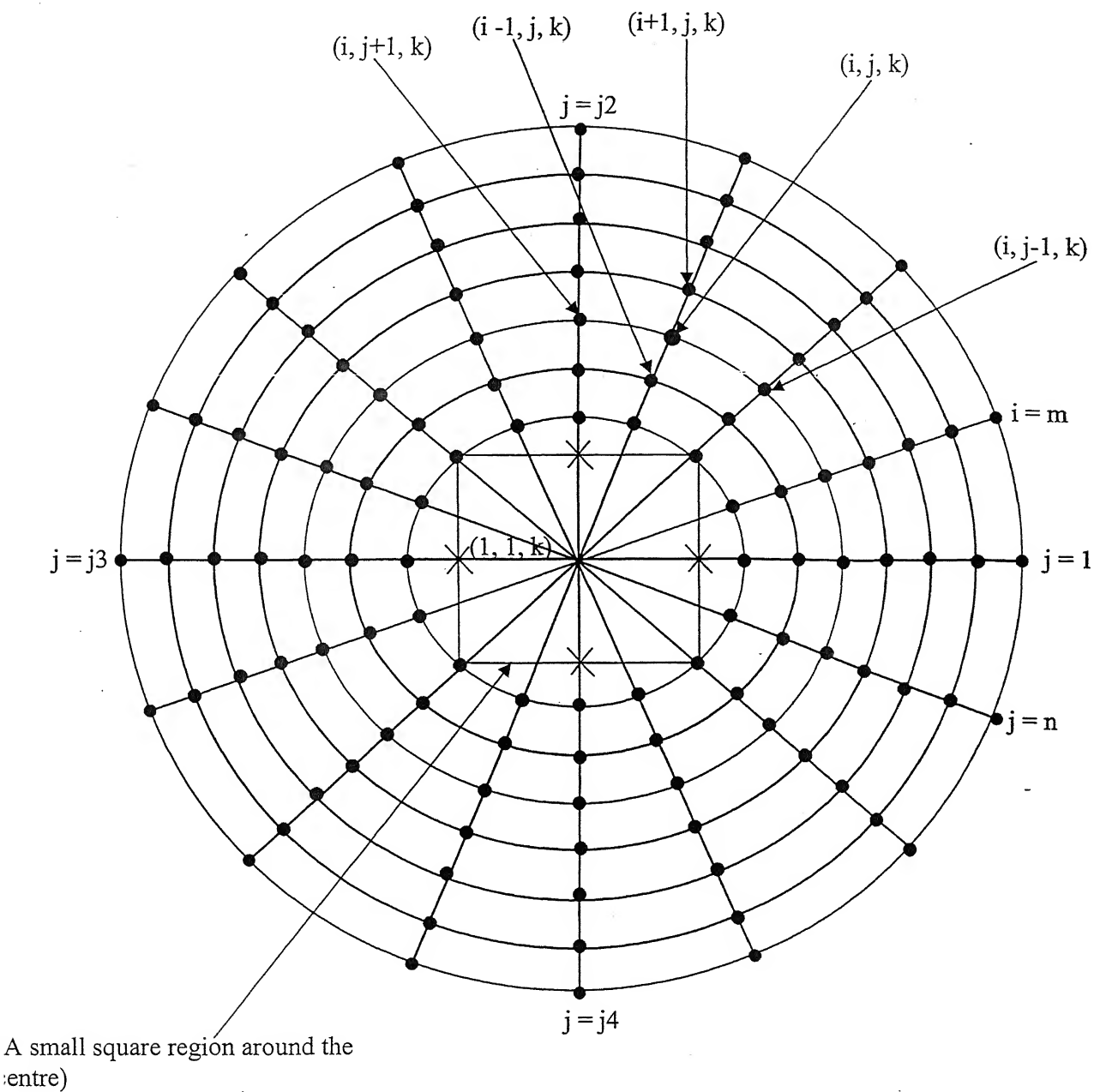
Fig. A.1 Grid in (r, θ) plane and pictorial representation of the treatment of the condition
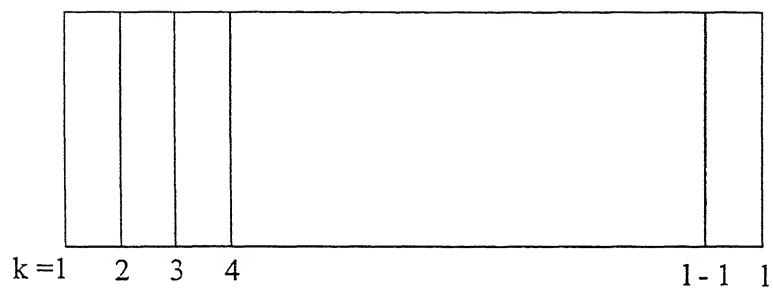
Fig. A,2 Grid lines in the axial direction (z)

APPENDIX B

Properties of Water and Propane as a function of pressure

The following are the best fit relation for various thermophysical properties as a function of pressure for water and propane. The data have been taken from EES (Engineering Equation Solver) for Water and Perry's Chemical Engineering Handbook for Propane.

B.1 Properties of liquid and vapour phases of water

1. Surface tension:

$$\sigma = (a + \exp(-c(p-b)))\,10^{-3} \tag{B.1}$$

Where,

$a = 2.4174$, $b = 0.0206$, $c = 192.5844$

σ is in N/m and p is in bar.

2. Latent Heat of Vapourization:

$$h_{fg} = a + b \exp\left(-\left(\frac{p-c}{d}\right)^2\right) \tag{B.2}$$

Where,

$a = -1216.0044$, $b = 2.933 \times 10^6$, $c = -4504.1362$, $d = 1731.561$

h_{fg} is in KJ/Kg and p is in bar.

3. Saturation Temperature:

$$T_{sat} = a\,p^3 + b\,p^2 + c\,p + d \tag{B.3}$$

Where,

$a = 7.4677 \times 10^{-5}$, $b = -0.0302$, $c = 4.2744$, $d = 394.8176$

T_{sat} is in Kelvin and p is in bar.

4. Specific Heat of liquid and vapour:

$$c_{p,l} = (a + \exp(c(p-b)))\tag{B.4}$$

Where,

$a = 5.3514$, $b = 168.4687$, $c = 0.0938$

$c_{p,l}$ is in KJ/Kg -K and p is in bar.

$$c_{p,v} = (a + \exp(c(p-b)))\tag{B.5}$$

Where,

$a = 2.524$, $b = 52.9461$, $c = 0.0241$

$c_{p,v}$ is in KJ/Kg -K and p is in bar.

5. Viscosity of liquid and vapour:

$$\mu_l = (a + b \exp(-(\frac{p-c}{d})^2) + e \exp(-(\frac{p-f}{g})^2)10^{-6}\tag{B.6}$$

Where,

$a = 65.2079$, $b = 1143.1998$, $c = -15.409$, $d = 11.0574$, $e = 118.0526$

$f = -81.0679$, $g = 127.1002$

μ_l is in N-s/m^2 and p is in bar.

$$\mu_v = (a + \exp(c(p-b)))\tag{B.7}$$

Where,

$a = 10.1242$, $b = -171.8871$, $c = 0.0084$

μ_v is in N-s/m^2 and.p is in bar.

6. Density of liquid and vapour:

$$\rho_l = (\frac{1}{a + b \exp(-((p-c)/d)^2)10^{-3}})\tag{B.8}$$

Where,

$a = 0.6558$, $b = 2.5818$, $c = 483.0463$, $d = 357.4776$

ρ_l is in Kg/m^3 and p is in bar.

$$\rho_v = (\frac{1}{a + \exp(-c(p-b))})$$ (B.9)

Where,

$a = 0.0562, b = 1.8681, c = 0.4723$

ρ_v is in Kg/m^3 and p is in bar.

7. Conductivity of liquid and vapour:

$$k_l = (a+b\ p)10^{-3}$$ (B.10)

Where,

$a = 686.5352, b = -1.583$

k_l is in W/m-K and p is in bar

$$k_v = (a + b\ p)10^{-3}$$ (B.11)

Where,

$a = 24.7355, b = 0.6088$

k_v is in W/m-K and p is in bar

In all the above expression the correlation coefficient varies between 0.9801 and 0.998.

B.2 Properties of liquid and vapour phases of propane

1. Surface tension:

$$\sigma = a + b\,p + c\,\exp(-p) \qquad\text{(B.21)}$$

Where,

$$a = .0113, b = -0.0004, = 0.1492$$

σ is in N/m and p is in bar.

2. Latent Heat of Vapourization:

$$h_{fg} = (a + b\,p + c\,p^2) \qquad\text{(B.22)}$$

Where,

$$a = 865.5829, b = 7.5152, c = -0.1596$$

h_{fg} is in KJ/Kg and p is in bar.

3. Saturation Temperature:

$$T_{sat} = (a + b\,p + c\,p^2)$$

(B.23)

Where,

$$a = 234.3563, b = 8.1314, c = -0.1608$$

T_{sat} is in Kelvin and p is in bar.

4. Specific Heat of liquid and vapour:

$$c_{p.l} = (a + b\,p + c\,p^2) \qquad\text{(B.24)}$$

Where,

$$a = 2.3097, b = 0.0364, c = 0.0007$$

$c_{p,l}$ is in KJ/Kg- K and p is in bar.

$$c_{p,v} = (a + b\,p) \qquad\text{(B.25)}$$

Where,

$$a = 1.5294, b = 0.0613$$

$c_{p,v}$ is in KJ/Kg-K and p is in bar.

5. Viscosity of liquid and vapour:

$$\mu_l = (a + b \exp(-p) + c\, p)\, 10^{-4} \qquad \text{(B.26)}$$

Where,

$$a = 1.5172, b = 1.9121, c = -0.04$$

μ_l is in N-s/m^2 and p is in bar.

$$\mu_v = (a + b\, p + c\, p^2)\, 10^{-4} \qquad \text{(B.27)}$$

Where,

$$a = 0.0730, b = 0.0012, c = 0.000013$$

μ_v is in N-s/m^2 and p is in bar.

6. Density of liquid and vapour:

$$\rho_l = (a + b\, p + c \exp(-p)) \qquad \text{(B.28)}$$

Where,

$$a = 553.8787, b = -6.0358, c = 122.95$$

ρ_l is in Kg/m^3 and p is in bar.

$$\rho_v(k) = (a + b\, p) \qquad \text{(B.29)}$$

Where,

$$a = -2.0782, b = 2.4746$$

ρ_v is in Kg/m^3 and p is in bar.

6. Conductivity of liquid and vapour:

$$k_l = (a + b\,p + c \exp(-p))$$ (B.30)

Where,

$$a = 0.1098, b = -0.0016, c = 0.0762$$

k_l is in W/m-K and p is in bar

$$k_v = (a + b\,p + c\,p^2)$$ (B.31)

Where,

$$a = 0.0115, b = 0.00101, c = -0.000015$$

k_v is in W/m-K and p is in bar

In the all above expressions the correlation coefficient various between 0.98 and 0.998.

REFERENCES

1. Bird, R.Byron, Steoart, Warren E., and Light foot, Edwin N., *"Transport Phenomena"*, Wiley International Edition, John Wily s Sons, New York, 1960.

2. Coiller, J.G.,*"Convective Boiling and Condensation"*, McGraw-Hill, 1972.

3. Ellepola, J. and Kenning, D., Nucleation site interactions in pool boiling. In *"Proceedings of the 2nd European Thermal sciences and 14th UK National Heat Transfer Conference"*, Rome, Italy, 1996.

4. Engineering Equation Solver (EES), Thermodynamic Property Data, Software, Academic Version 6. 036, USA, 1992 – 2000.

5. Fox, Robert W. and Mc Donald, Alan J., *" Introduction to Fluid Mechanics"*, 4th Ed., John Wiley s Sons, New York, 1995.- 2000.

6. Ghoshdastidar, P.S., Kabelac, S., and Mohanty, A., *" Numerical modelling of atmospheric pool boiling by The coupled map lattice method"*, J. Mechanical Engineering Science I Mech.E Part C, Vol. 218, pp. 195 – 205, 2004.

7. Ghoshdastidar, P. S., *"Heat Transfer"*, Oxford University Press, 2004.

8. Kaneko, K., *Theory and application of Coupled Map Lattices*, John wiley, Chichester, 1993.

9. Nelson, R., Kenning, D. and Shoji, M., *"Nonlinear effects and behavior in nucleate boiling"* In *4th Experimental Chaos Conference,* Boca Raton, Florida, 6-8 August 1997.

10. Perry, Robert H. and Green, Donald W., *"Perry's Chemical Engineers' Hand book"*, 7th Ed., Mc Graw-Hill, New York, 1997.

11. Sadasivan, P., Unal, C. and Nelson, R. A., *"Nonlinear aspects of high heat flux nucleate boiling heat transfer"*, *Report LA-UR-95-609*, 1995.

12. Shoji, M. and Tajima, K., *"Mathematical simulation model of boiling: modes and chaos"* In *Convective Flow and Pool Boiling Conference*, May 18-23, Kloster Irsee, Germany, 18-23 May 1997.

13. Shoji, M., *"Boiling simulator – a simple theoretical model of boiling"*, In *Third International Conference on Multiphase Flow*, Lyon, France, 8-12 June 1998.

15. Stephan, Karl, *Heat Transfer in Condensation and Boiling*, Springer-Verlag, Berlin, 1992.

16. Wang, C.H. and Dhir, V.K., "*Effect of surface wettability on active nucleation site density*", *Trans. ASME, J. Heat Transfer*, Vol. 115, 659-669, 1993.

17. Yanagita, T. and Kaneko, K., "*Coupled map lattice model for convection*", *Physics Lett. A*, Vol. 175, 415-420, 1993.

18. Yanagita, T., "*Phenomenology for boiling: a coupled map lattice model*", *Chaos*, , Vol. 2, 343-350,1992